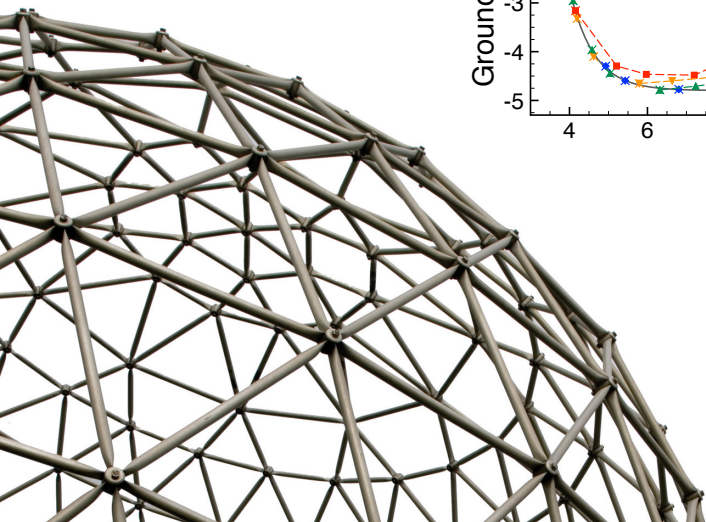
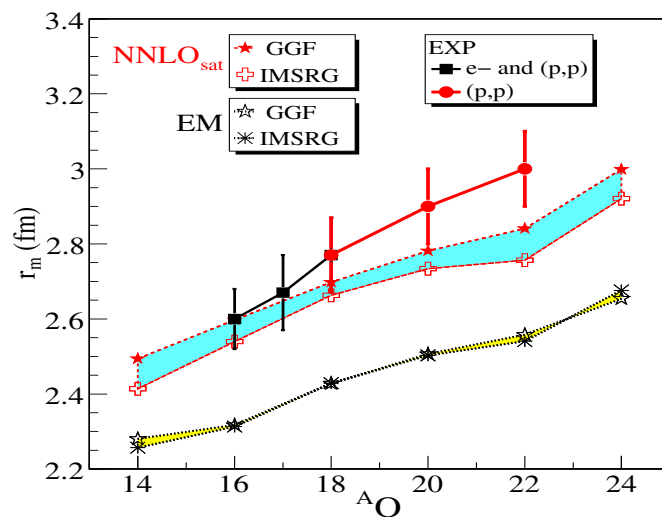
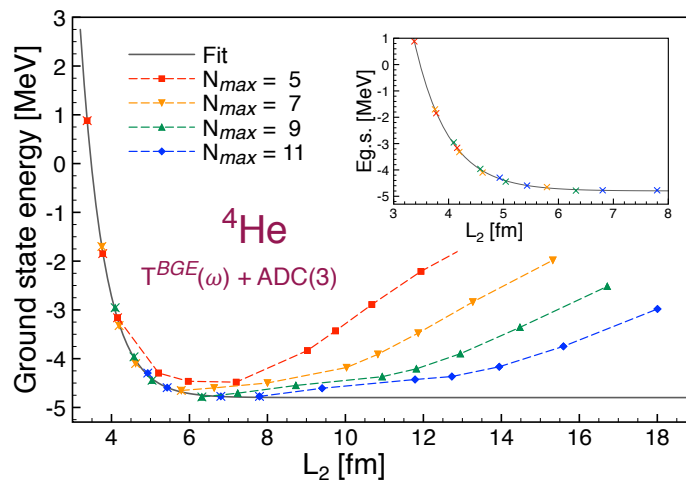


SCGF Computations of Nuclei

Carlo Barbieri — University of Surrey

16 May 2017



Current Status of low-energy nuclear physics

Composite system of interacting fermions

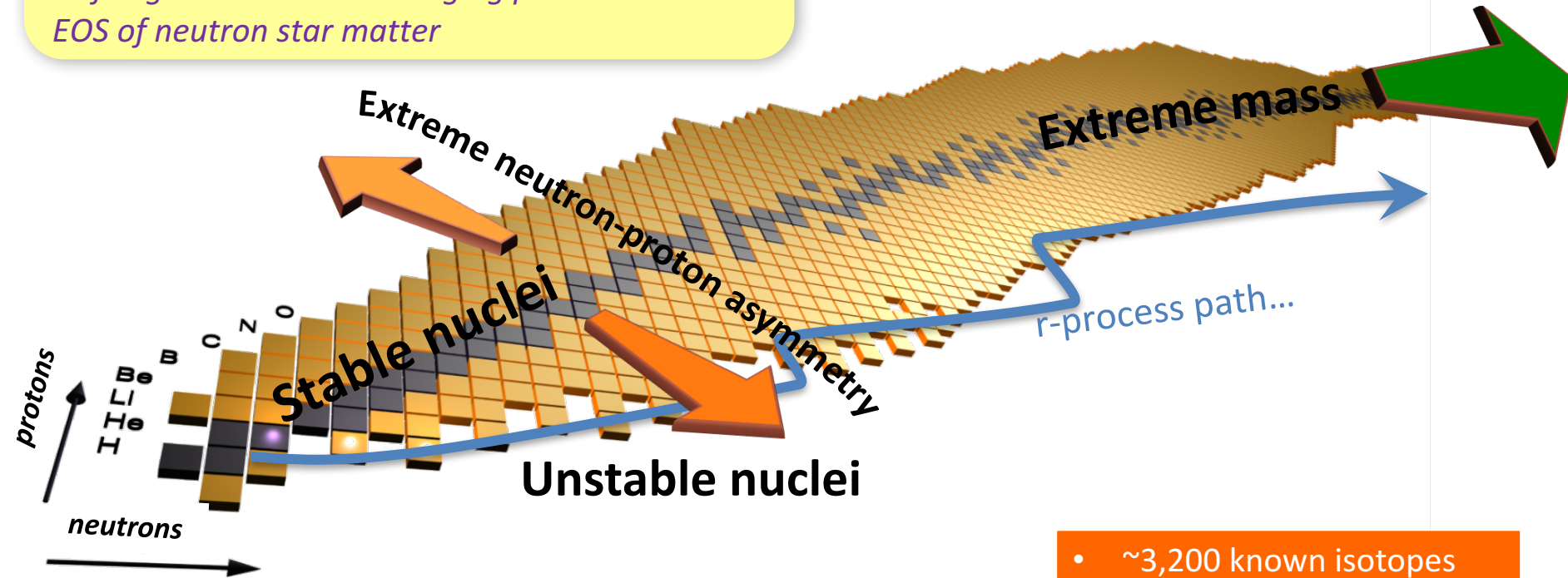
Binding and limits of stability

Coexistence of individual and collective behaviors

Self-organization and emerging phenomena

EOS of neutron star matter

Experimental
programs
RIKEN, FAIR, FRIB

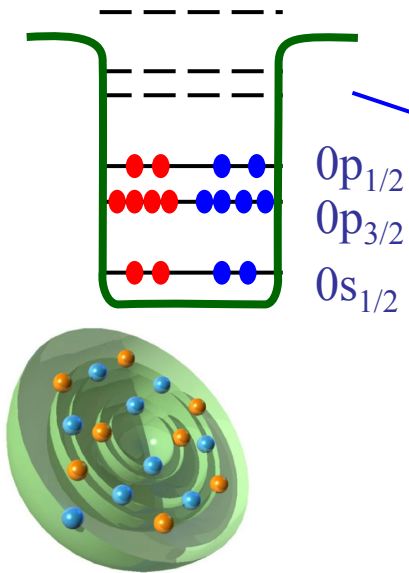


- ~3,200 known isotopes
- ~7,000 predicted to exist
- Correlation characterised in full for ~283 stable

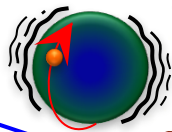
Nature **473**, 25 (2011); **486**, 509 (2012)

Concept of correlations

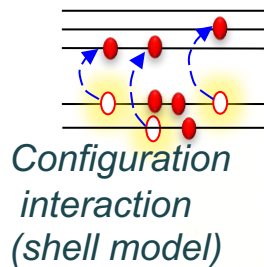
independent
particle picture



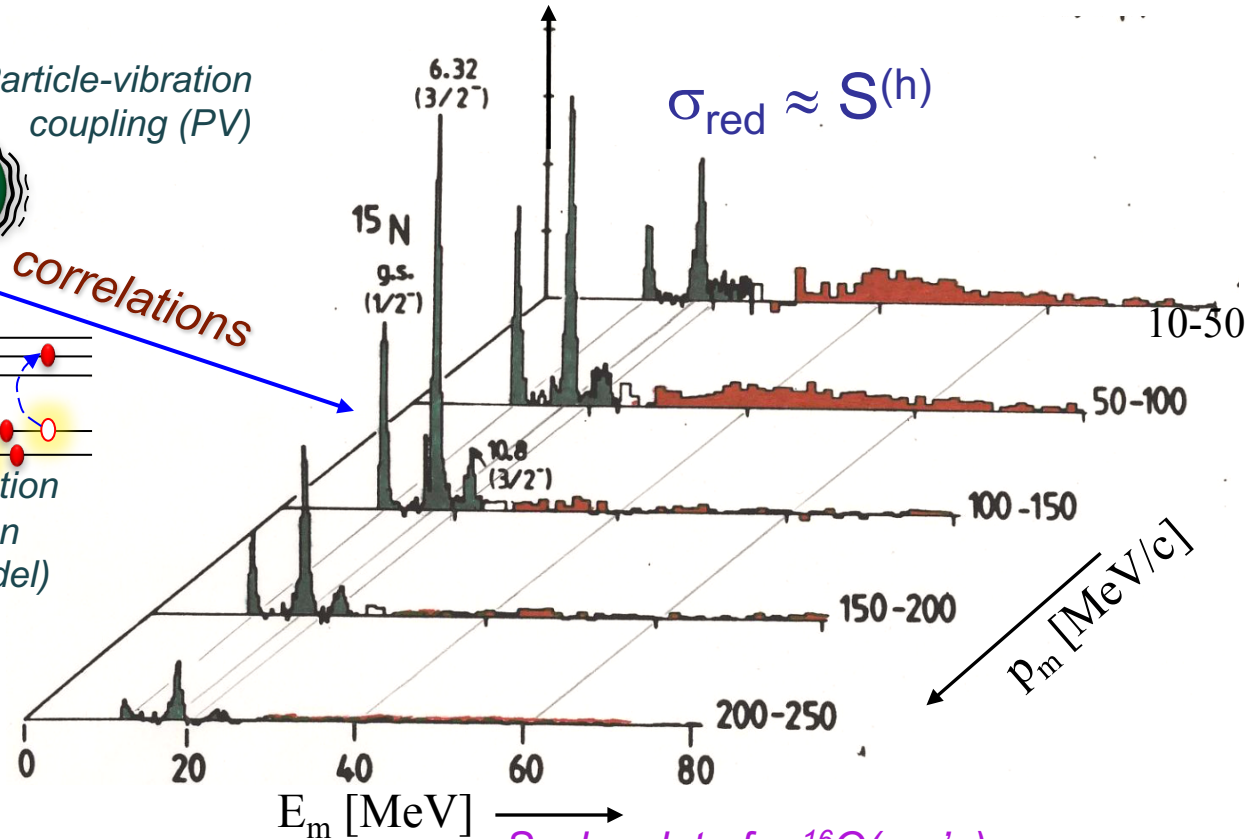
Particle-vibration
coupling (PV)



correlations



Spectral function: distribution of
momentum (p_m) and energies (E_m)



Saclay data for $^{16}\text{O}(e,e'p)$

[Mougey et al., Nucl. Phys. A335, 35 (1980)]

Understood for a few stable closed shells:

[CB and W. H. Dickhoff, Prog. Part. Nucl. Phys 52, 377 (2004)]

Concept of correlations

independent
particle picture

Spectral function: distribution of
momentum (p_m) and

Particle-vibration
coupling

Want to understand structure and nuclear forces
directly from first principles (ab initio).

So far, fully characterised only for closed-shell and
stable isotopes... (!)

[W. Dickhoff, CB, Prog. Part. Nucl. Phys. **52**, 377 (2004)]

E_m [MeV] → 60 80 200-250

Saclay data for $^{16}\text{O}(e,e'p)$

[Mougey et al., Nucl. Phys. A335, 35 (1980)]

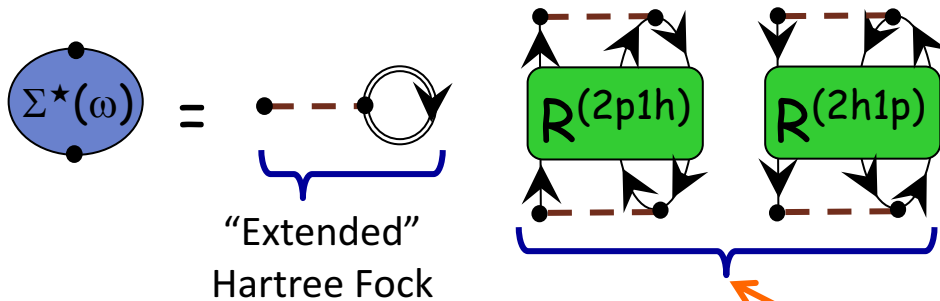
Understand a few stable closed shells:

[CB and W. H. Dickhoff, Prog. Part. Nucl. Phys **52**, 377 (2004)]

The FRPA Method in Two Words

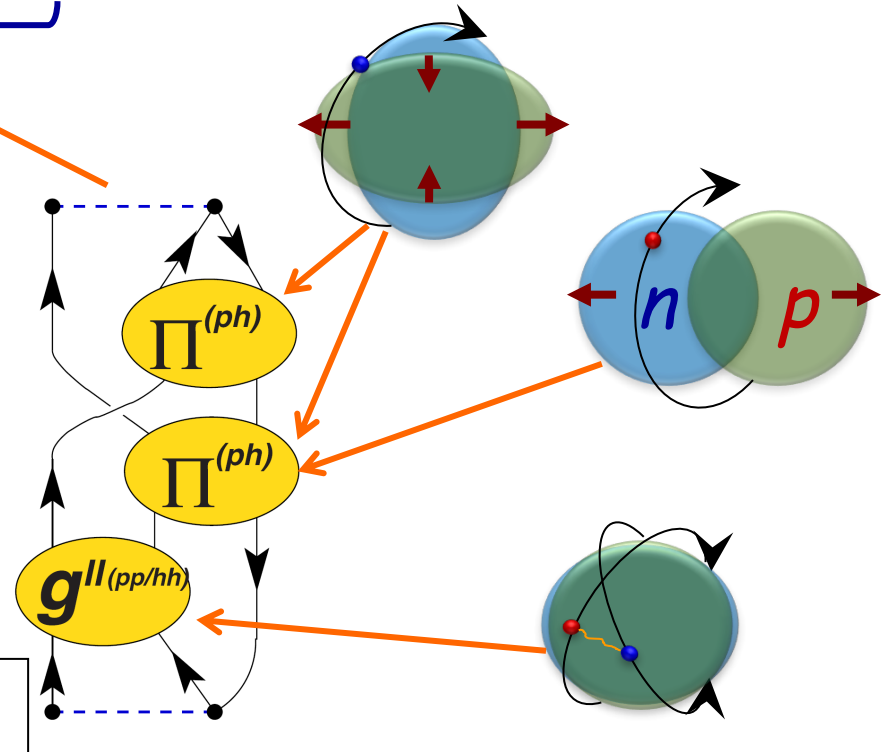
Particle vibration coupling is the main cause driving the distribution of particle strength—on both sides of the Fermi surface...

CB et al.,
 Phys. Rev. C63, 034313 (2001)
 Phys. Rev. A76, 052503 (2007)
 Phys. Rev. C79, 064313 (2009)

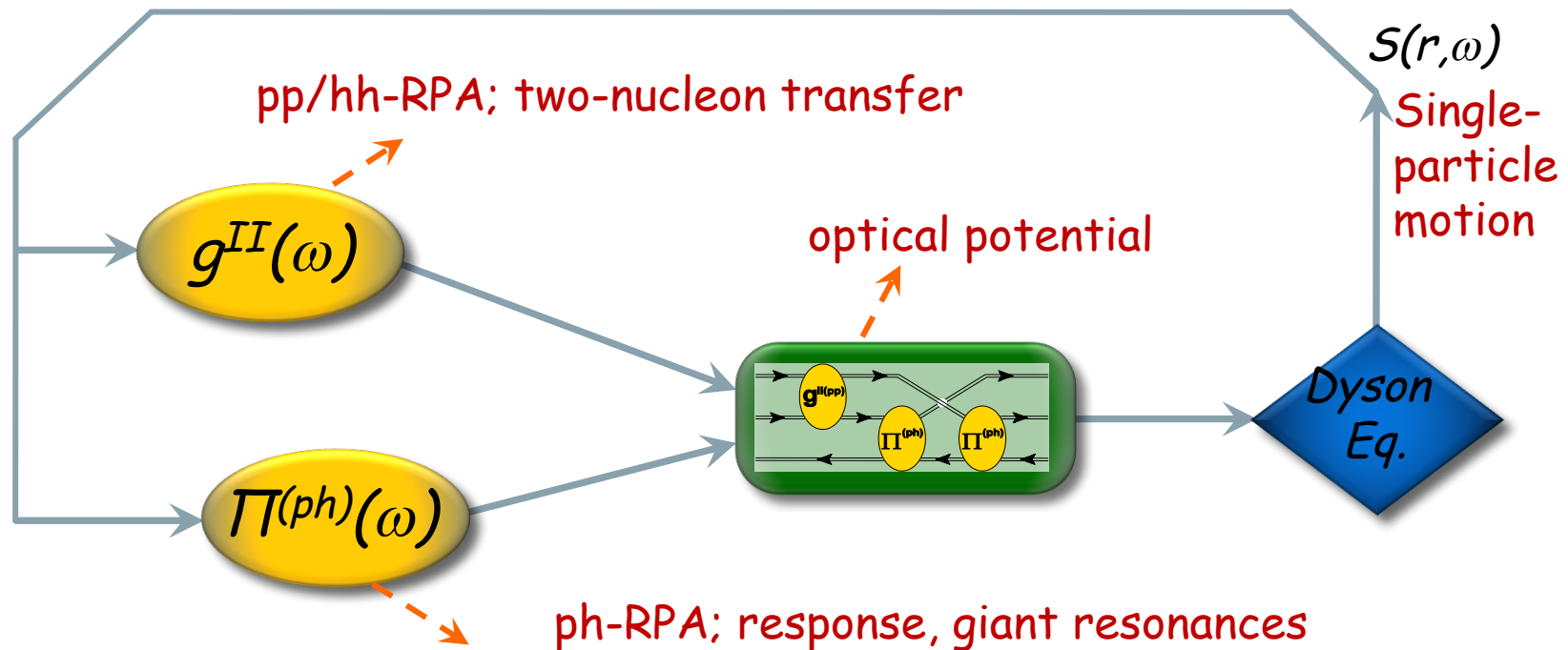


- A complete expansion requires all types of particle-vibration coupling
 ...these modes are all resummed exactly and to all orders in a *ab-initio* many-body expansion.

- The Self-energy $\Sigma^*(\omega)$ yields both single-particle states and scattering

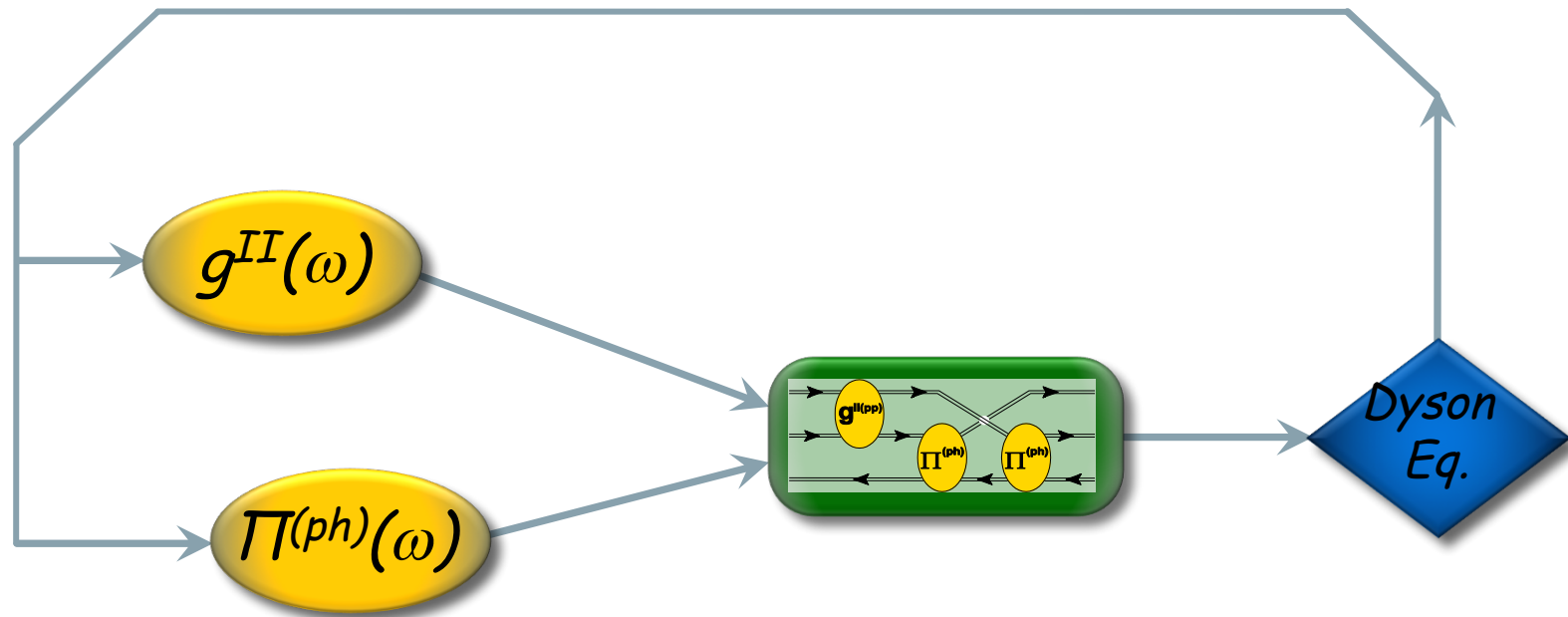


Self-Consistent Green's Function Approach



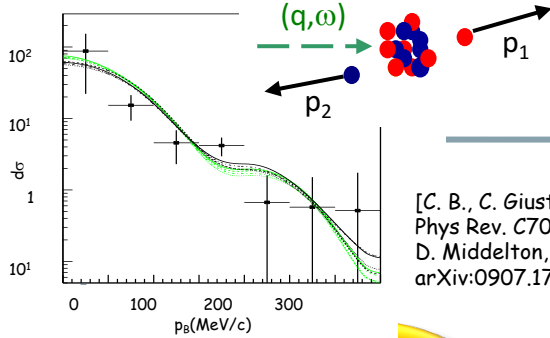
- Global picture of nuclear dynamics
- Reciprocal correlations among effective modes
- Guaranties *macroscopic conservation laws*

Self-Consistent Green's Function Approach

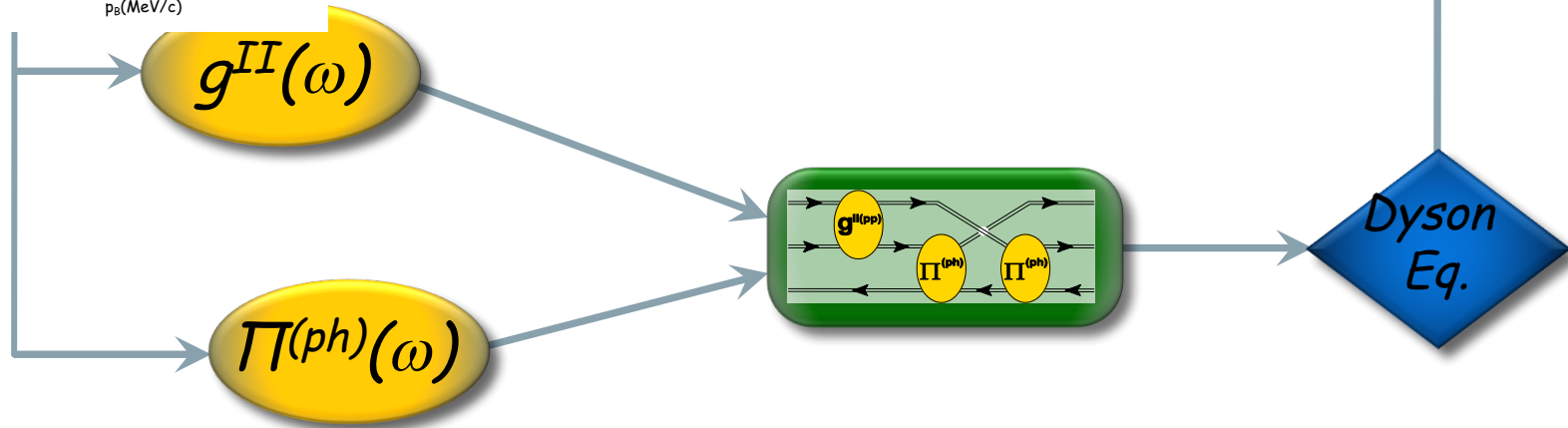


Self-Consistent Green's Function Approach

$^{16}\text{O}(e,e'pn)^{14}\text{N}$ @ MAINZ

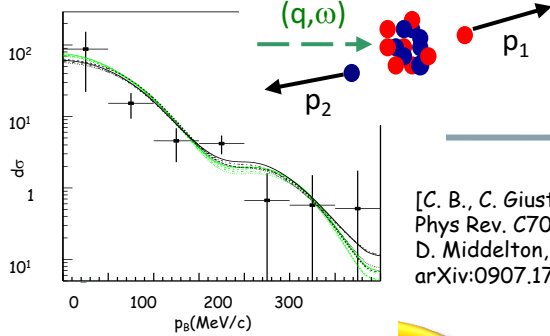


[C. B., C. Giusti, et al.
Phys Rev. C70, 014606 (2004)
D. Middleton, et al.
arXiv:0907.1758; EPJA in print]



Self-Consistent Green's Function Approach

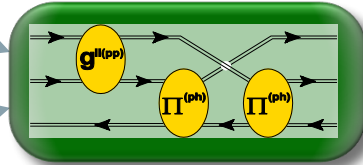
$^{16}\text{O}(e,e'pn)^{14}\text{N}$ @ MAINZ



[C. B., C. Giusti, et al.
Phys Rev. C70, 014606 (2004)
D. Middleton, et al.
arXiv:0907.1758; EPJA in print]

$$g^{II}(\omega)$$

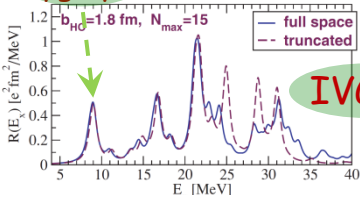
$$\Pi^{(ph)}(\omega)$$



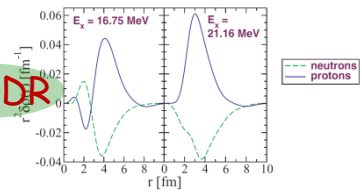
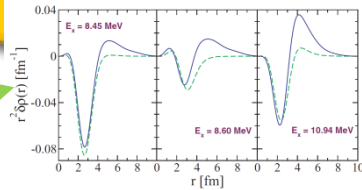
Dyson Eq.

Isovector response for ^{32}Ar , ^{34}Ar

Proton Pygmy



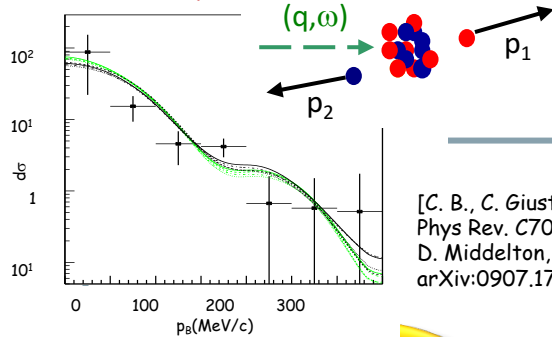
IVGDR



[C. B., K. Langanke, et al., Phys Rev. C77, 024304 (2008)]

Self-Consistent Green's Function Approach

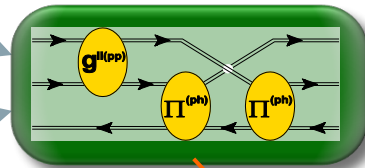
$^{16}\text{O}(e,e'pn)^{14}\text{N}$ @ MAINZ



[C. B., C. Giusti, et al.
Phys Rev. C70, 014606 (2004)
D. Middleton, et al.
arXiv:0907.1758; EPJA in print]

$$g^{II}(\omega)$$

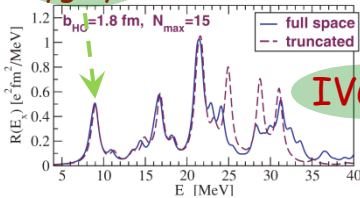
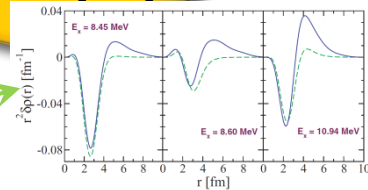
$$\Pi^{(ph)}(\omega)$$



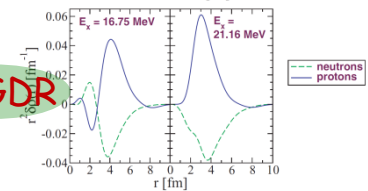
Dyson Eq.

Isovector response for ^{32}Ar , ^{34}Ar

Proton Pygmy



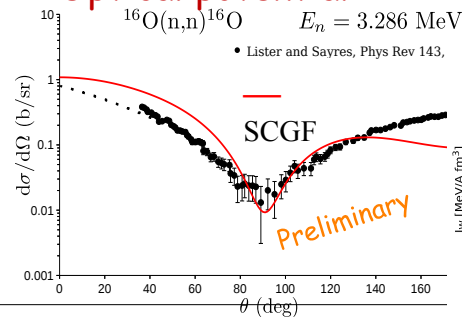
IVGDR



Optical potential

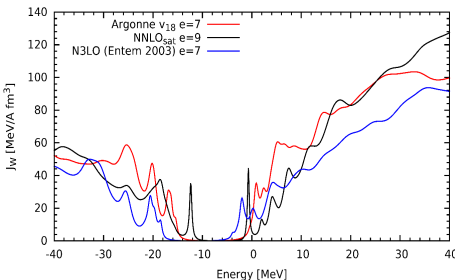
$^{16}\text{O}(n,n)^{16}\text{O}$ $E_n = 3.286$ MeV

• Lister and Sayres, Phys Rev 143,



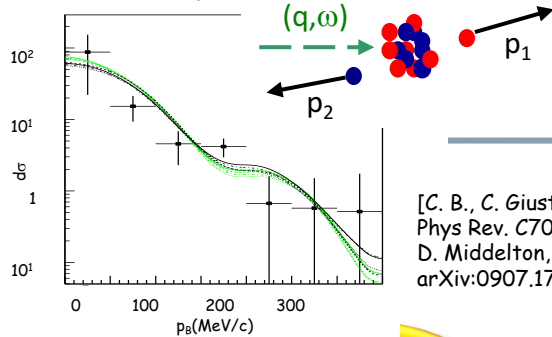
See talk of A. Idini and arXiv:1612.01478 [nucl-th]

^{48}Ca neutrons



Self-Consistent Green's Function Approach

$^{16}\text{O}(e,e'pn)^{14}\text{N}$ @ MAINZ

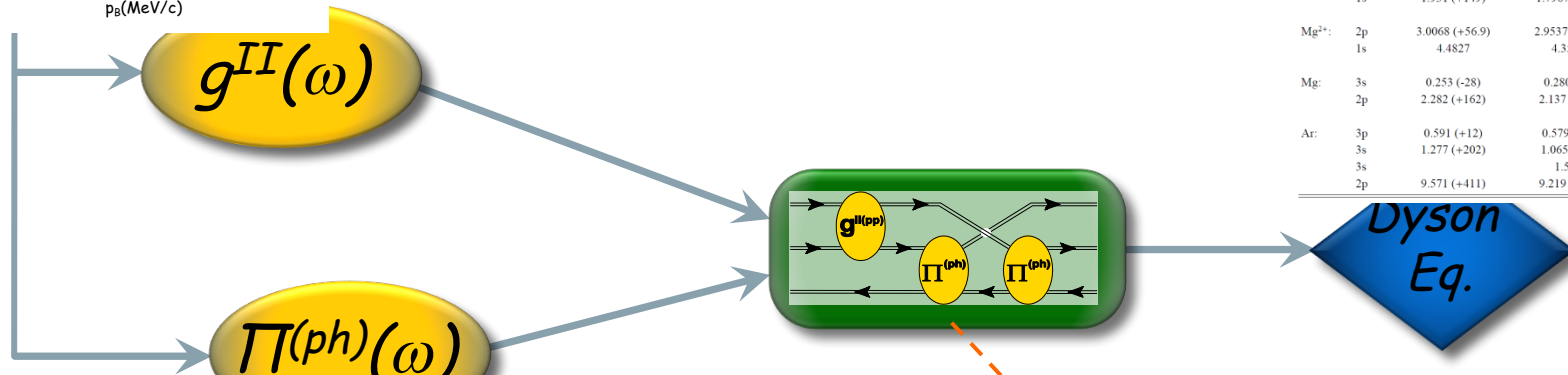


[C. B., C. Giusti, et al.
Phys Rev. C70, 014606 (2004)
D. Middleton, et al.
arXiv:0907.1758; EPJA in print]

**Ionization energies/
affinities, in atoms**

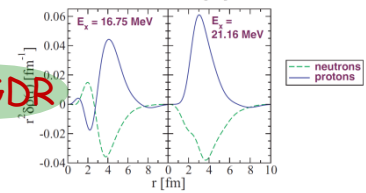
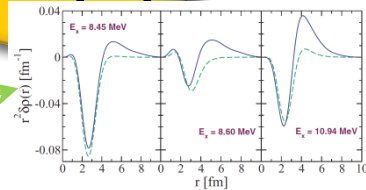
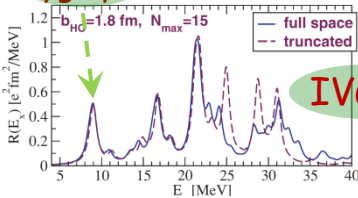
[CB, D. Van Neck,
AIP Conf.Proc.1120,104 ('09) & in prep]

		Hartree-Fock	FRPAc	Experiment [16, 17]
He:	1s	0.918 (+14)	0.9008 (-2.9)	0.9037
Be ²⁺ :	1s	5.6672 (+116)	5.6551 (-0.5)	5.6556
Be:	2s	0.3093 (-34)	0.3224 (-20.2)	0.3426
	1s	4.733 (+200)	4.5405 (+8)	4.533
Ne:	2p	0.852 (+57)	0.8037 (+11)	0.793
	1s	1.931 (+149)	1.7967 (+15)	1.782
Mg ²⁺ :	2p	3.0068 (+56.9)	2.9537 (+3.8)	2.9499
	1s	4.4827	4.3589	
Mg:	3s	0.253 (-28)	0.280 (-1)	0.281
	2p	2.282 (+162)	2.137 (+17)	2.12
Ar:	3p	0.591 (+12)	0.579 (=0)	0.579
	3s	1.277 (+202)	1.065 (-10)	1.075
	3s		1.544	
	2p	9.571 (+411)	9.219 (+59)	9.160



**Isovector response
for ^{32}Ar , ^{34}Ar**

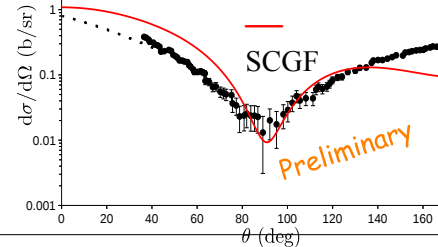
**Proton
Pygmy**



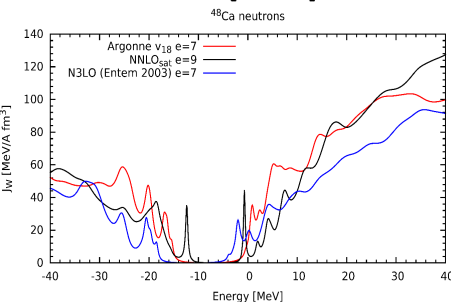
Optical potential

$^{16}\text{O}(n,n)^{16}\text{O}$ $E_n = 3.286$ MeV

• Lister and Sayres, Phys Rev 143,

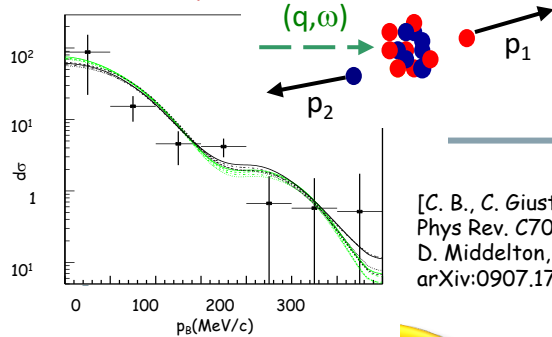


See talk of A.Idini and
arXiv:1612.01478 [nucl-th]



Self-Consistent Green's Function Approach

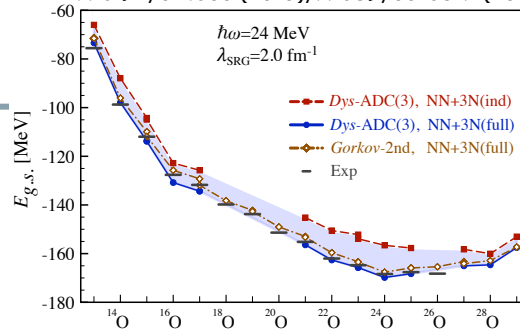
$^{16}\text{O}(e,e'pn)^{14}\text{N}$ @ MAINZ



[C. B., C. Giusti, et al. Phys Rev. C70, 014606 (2004)
D. Middleton, et al. arXiv:0907.1758; EPJA in print]

Binding energies

[PRL. 111, 062501 (2013),
PRC 92, 014306 (2015), PRC89, 061301R (2014)]



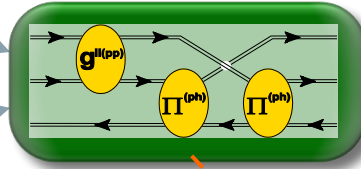
Ionization energies/
affinities, in atoms

[CB, D. Van Neck,
AIP Conf.Proc.1120,104 ('09) & in prep]

		Hartree-Fock	FRPAc	Experiment [16, 17]
He:	1s	0.918 (+14)	0.9008 (-2.9)	0.9037
Be ²⁺ :	1s	5.6672 (+116)	5.6551 (-0.5)	5.6556
Be:	2s	0.3093 (-34)	0.3224 (-20.2)	0.3426
	1s	4.733 (+200)	4.5405 (+8)	4.533
Ne:	2p	0.852 (+57)	0.8037 (+11)	0.793
	1s	1.931 (+149)	1.7967 (+15)	1.782
Mg ²⁺ :	2p	3.0068 (+56.9)	2.9537 (+3.8)	2.9499
	1s	4.4827	4.3589	
Mg:	3s	0.253 (-28)	0.280 (-1)	0.281
	2p	2.282 (+162)	2.137 (+17)	2.12
Ar:	3p	0.591 (+12)	0.579 (±0)	0.579
	3s	1.277 (+202)	1.065 (-10)	1.075
	3s		1.544	
	2p	9.571 (+411)	9.219 (+59)	9.160

$g^{II}(\omega)$

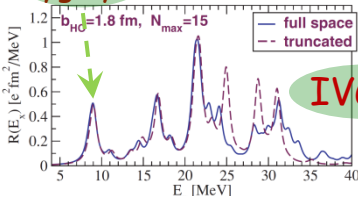
$\Pi(ph)(\omega)$



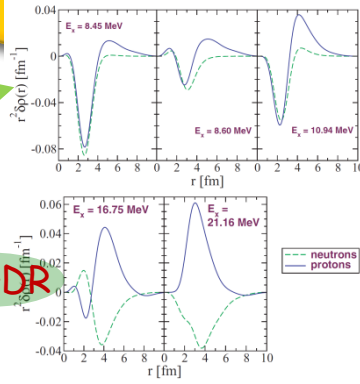
Dyson Eq.

Isovector response
for ^{32}Ar , ^{34}Ar

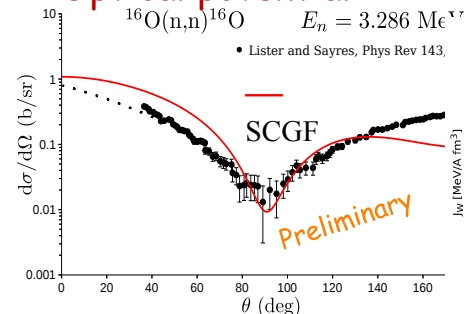
Proton
Pygmy



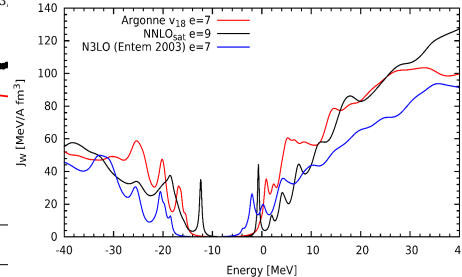
IVGDR



Optical potential



arXiv:1612.01478 [nucl-th]



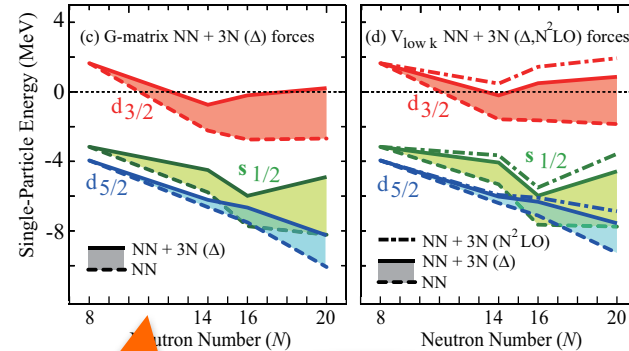
Modern realistic nuclear forces

Chiral EFT for nuclear forces:

	2N forces	3N forces	4N forces
LO $\mathcal{O}\left(\frac{Q^0}{\Lambda^0}\right)$			
NLO $\mathcal{O}\left(\frac{Q^2}{\Lambda^2}\right)$			
N ² LO $\mathcal{O}\left(\frac{Q^3}{\Lambda^3}\right)$			
N ³ LO $\mathcal{O}\left(\frac{Q^4}{\Lambda^4}\right)$			

(3NFs arise naturally at N2LO)

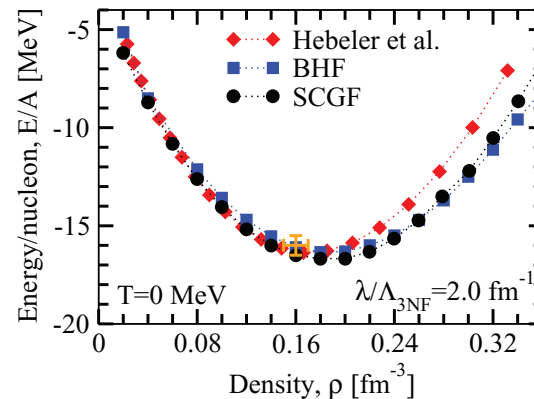
Single particle spectrum at E_{fermi} :



[T. Otsuka et al., Phys. Rev. Lett **105**, 032501 (2010)]

Need at LEAST 3NF!!!
("cannot" do RNB physics without...)

Saturation of nuclear matter:



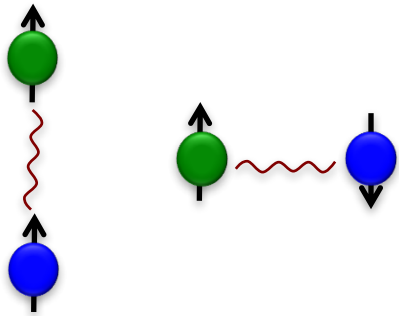
[A. Carbone et al., Phys. Rev. C **88**, 044302 (2013)]

Nuclear forces in exotic nuclei

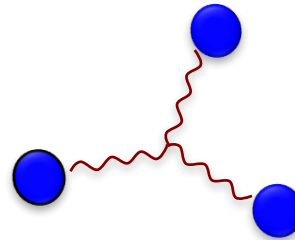
Nucleon interactions are very complex and difficult to handle...

Symmetric matter:
 $N \approx Z$

Tensor force (p-n)



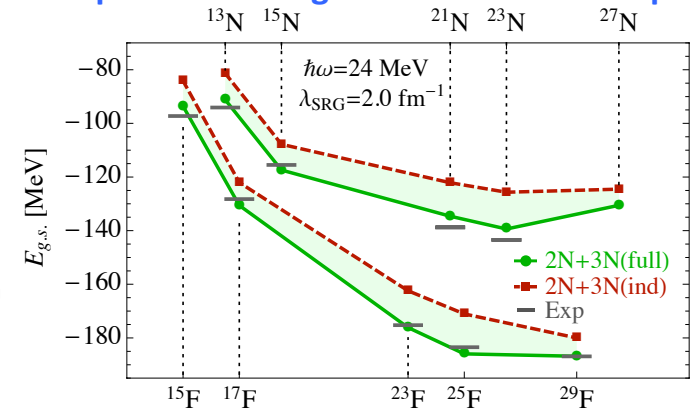
Three-nucleon Force (3NF)



Neutron-rich matter ($N \gg Z$):

- Neutron star matter EoS
- Symmetry energy
- new shell closures

Drip-lines of nitrogen and fluorine isotopes



[A. Cipollone, CB, P. Navrátil, Phys. Rev. Lett. **111**, 062501 (2013)]

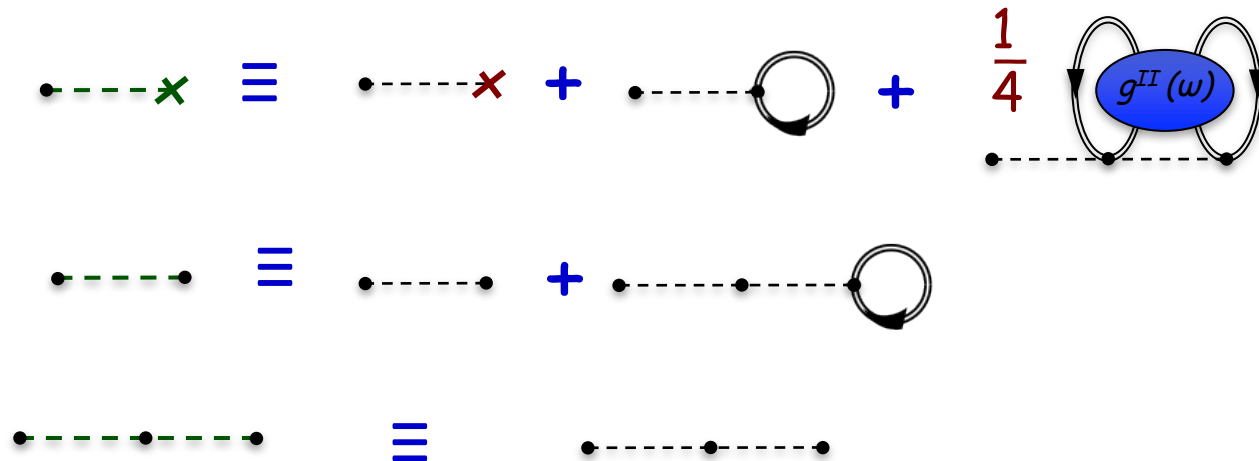
Change of regime from
stable to dripline isotopes !

Inclusion of NNN forces

A. Carbone, CB, et al., Phys. Rev. C88, 054326 (2013)

- NNN forces can enter diagrams in three different ways:

→ Define new 1- and 2-body interactions and use only interaction-irreducible diagrams

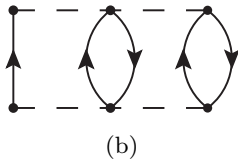
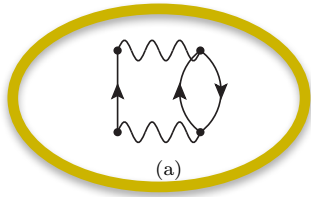


- Contractions are with fully correlated density matrices (BEYOND a normal ordering...)

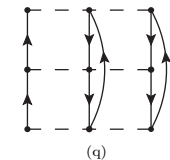
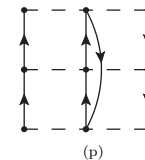
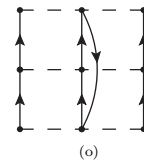
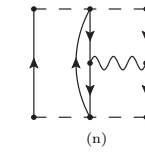
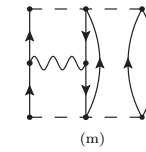
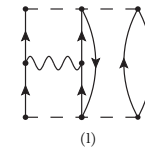
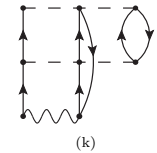
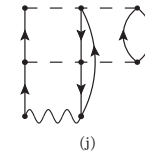
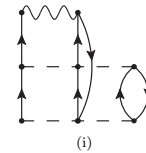
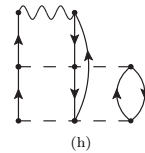
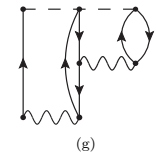
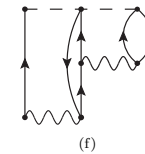
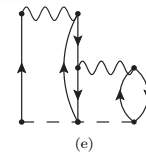
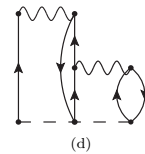
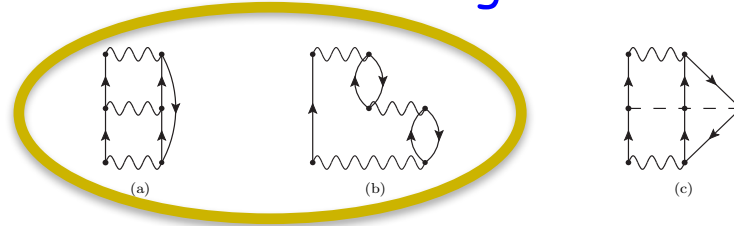
Inclusion of NNN forces

A. Carbone, CB, et al., *Phys. Rev. C* **88**, 054326 (2013)
and F. Raimondi, CB, arXiv:1709.04330 PRC (2017).

- Second order PT diagrams with 3BFs:



- Third order PT diagrams with 3BFs:



→ Use of irreducible 2-body interactions

→ Need to correct the Koltun sum rule (for energy)

→ 3p2h/3h2p terms relevant to next-generation high-precision methods.

FIG. 5. 1PI, skeleton and interaction irreducible self-energy diagrams appearing at 3^{rd} -order in perturbative expansion (7), making use of the effective hamiltonian of Eq. (9).

Inclusion of NNN forces

→ 3p2h/3h2p terms relevant to next-generation high-precision methods.

ADCH) formalism is

$$M^{ADCH(0)} = M^{ADCH(0)} + M^{(10)} + M^{(20)} + M^{(30)} + M^{(40)} + M^{(50)} + M^{(60)} + M^{(70)} + M^{(80)} + M^{(90)} + M^{(100)}$$

$$+ M^{(110)} + M^{(120)} + M^{(130)} + M^{(140)} + M^{(150)} + M^{(160)} + M^{(170)} + M^{(180)} + M^{(190)} + M^{(200)}$$

$$N^{ADCH(0)} = N^{ADCH(0)} + N^{(10)} + N^{(20)} + N^{(30)} + N^{(40)} + N^{(50)} + N^{(60)} + N^{(70)} + N^{(80)} + N^{(90)} + N^{(100)}$$

$$+ N^{(110)} + N^{(120)} + N^{(130)} + N^{(140)} + N^{(150)} + N^{(160)} + N^{(170)} + N^{(180)} + N^{(190)} + N^{(200)}$$

$$C_{ij} = C_{ij}^{(0)} + C_{ij}^{(10)} + C_{ij}^{(20)} + C_{ij}^{(30)} + C_{ij}^{(40)} + C_{ij}^{(50)} + C_{ij}^{(60)} + C_{ij}^{(70)} + C_{ij}^{(80)} + C_{ij}^{(90)} + C_{ij}^{(100)}$$

$$+ C_{ij}^{(110)} + C_{ij}^{(120)} + C_{ij}^{(130)} + C_{ij}^{(140)} + C_{ij}^{(150)} + C_{ij}^{(160)} + C_{ij}^{(170)} + C_{ij}^{(180)} + C_{ij}^{(190)} + C_{ij}^{(200)}$$

$$D_{ij} = D_{ij}^{(0)} + D_{ij}^{(10)} + D_{ij}^{(20)} + D_{ij}^{(30)} + D_{ij}^{(40)} + D_{ij}^{(50)} + D_{ij}^{(60)} + D_{ij}^{(70)} + D_{ij}^{(80)} + D_{ij}^{(90)} + D_{ij}^{(100)}$$

$$+ D_{ij}^{(110)} + D_{ij}^{(120)} + D_{ij}^{(130)} + D_{ij}^{(140)} + D_{ij}^{(150)} + D_{ij}^{(160)} + D_{ij}^{(170)} + D_{ij}^{(180)} + D_{ij}^{(190)} + D_{ij}^{(200)}$$

For the coupling matrices M_{ij} and N_{ij} , the list of terms represented at the ADCH) level is composed by sets of ADC(1) terms, defined in Eqs. (18, 36) and in Eqs. (18, 27) for the forward-in-time and backward-in-time self-energy respectively; sets of terms from (H) to (I) appearing at third order of the ADC, presented in Eqs. (12, 28, 56) and in Eqs. (54, 55, 57), which contain only 2p1h and 2h1p configurations; and those terms from (H) to (I) with 2p1h and 2h1p ISCs introduced in Eqs. (66-68, 74-77) in Eqs. (70-73, 78-81). Other terms with 2p1h and 2h1p ISCs, denoted with superscripts from (H) to (I) as defined in Eqs. (A5-A20) below. Moreover, in Eqs. (A1-A2) we list additional terms that need to be added to the ADC(1) when the single-particle propagator used to construct self-energy diagrams is uncontracted, i.e. when one works with a non-skeleton expansion. For coupling matrices, these additional terms are identical with superscripts ranging from (H) to (I). Their explicit expressions will be given in Appendix C.2.

Interaction matrices appear at third order in the ADC, as listed in Eqs. (A3-A4). The first three terms listed concerning to 2p1h and 2h1p configurations, are given in Eqs. (C8-C9, C2) for forward-in-time diagrams and in Eqs. (C6, 8), (C3) for backward-in-time ones. Other matrices required to link 3p2h/3h2p ISCs are denoted by $C_{ij}^{(30)}, \dots, C_{ij}^{(200)}$, $D_{ij}^{(30)}, \dots, D_{ij}^{(200)}$. These will be given later in Eqs. (A21-A24), (A25-A28), (A29-A30), (A31-A34). Finally, additional four interaction matrices introduced in Appendix C.2 for the non-skeleton expansion are specified in Eqs. (A3-A4) through the

1. Coupling matrices

In Fig. 5c we list

$$N^{(30)} = \Delta(j_1, j_2, j_3, j_4) \Delta(j_1, j_2, j_3, j_4) \sum_{j_5, j_6} \sum_{j_7, j_8} \Delta(j_5, j_6, j_7, j_8) \Delta(j_5, j_6, j_7, j_8)$$

$$\times (-1)^{j_1+j_2+j_3+j_4+j_5+j_6+j_7+j_8} \frac{d_{j_5, j_6, j_7, j_8}}{2j_5+1} \sqrt{1+d_{j_5, j_6, j_7, j_8}}$$

$$\times \left(\frac{A_{j_5, j_6, j_7, j_8}^{(30)}}{2j_5+1} \sqrt{1+d_{j_5, j_6, j_7, j_8}} - (-1)^{j_1+j_2+j_3+j_4} A_{j_5, j_6, j_7, j_8}^{(30)} \sqrt{1+d_{j_5, j_6, j_7, j_8}} \right) \left(\frac{A_{j_5, j_6, j_7, j_8}^{(30)}}{2j_5+1} \sqrt{1+d_{j_5, j_6, j_7, j_8}} \right)_{j_5, j_6, j_7, j_8, j_5, j_6, j_7, j_8}^{(30)}$$

2. Coupling matrices

Diagram in backslash (B) is obtained from Fig. 5a for the forward

Finally, the coupling matrix $N^{(30)}$ of Eq. (57) is found in the backward-in-time diagram of Fig. 2c and contains a 1NF. It has the following form in the angular momentum coupling representation,

$$N^{(30)} = \Delta(j_1, j_2, j_3, j_4) \Delta(j_1, j_2, j_3, j_4) \sum_{j_5, j_6} \sum_{j_7, j_8} \Delta(j_5, j_6, j_7, j_8) \Delta(j_5, j_6, j_7, j_8)$$

$$\times (-1)^{j_1+j_2+j_3+j_4+j_5+j_6+j_7+j_8} \frac{d_{j_5, j_6, j_7, j_8}}{2j_5+1} \sqrt{1+d_{j_5, j_6, j_7, j_8}}$$

$$\times \left(\frac{A_{j_5, j_6, j_7, j_8}^{(30)}}{2j_5+1} \sqrt{1+d_{j_5, j_6, j_7, j_8}} - (-1)^{j_1+j_2+j_3+j_4} A_{j_5, j_6, j_7, j_8}^{(30)} \sqrt{1+d_{j_5, j_6, j_7, j_8}} \right) \left(\frac{A_{j_5, j_6, j_7, j_8}^{(30)}}{2j_5+1} \sqrt{1+d_{j_5, j_6, j_7, j_8}} \right)_{j_5, j_6, j_7, j_8, j_5, j_6, j_7, j_8}^{(30)}$$

Interaction matrices with 2p1h and 2h1p ISCs

The interaction matrix C_{ij} can contract 2p1h propagators through particle-particle, particle-hole and 2NFs, according to the terms

$$C_{ij} = C_{ij}^{(10)} + C_{ij}^{(20)} + C_{ij}^{(30)}$$

which have been introduced in Eqs. (20), (29) and (32), respectively.

The particle-hole interaction matrix results from the diagram in Fig. 2b. Using the angular momentum coupling of Eq. (B14) we have:

$$C_{ij}^{(10)} = \Delta(j_1, j_2, j_3, j_4) \Delta(j_1, j_2, j_3, j_4) \Delta(j_5, j_6, j_7, j_8) \Delta(j_5, j_6, j_7, j_8) \sum_{j_9, j_{10}} \sum_{j_{11}, j_{12}} \Delta(j_9, j_{10}, j_{11}, j_{12}) \Delta(j_9, j_{10}, j_{11}, j_{12})$$

$$\times \left(\frac{A_{j_9, j_{10}, j_{11}, j_{12}}^{(10)}}{2j_9+1} \sqrt{1+d_{j_9, j_{10}, j_{11}, j_{12}}} - (-1)^{j_1+j_2+j_3+j_4} A_{j_9, j_{10}, j_{11}, j_{12}}^{(10)} \sqrt{1+d_{j_9, j_{10}, j_{11}, j_{12}}} \right) \left(\frac{A_{j_9, j_{10}, j_{11}, j_{12}}^{(10)}}{2j_9+1} \sqrt{1+d_{j_9, j_{10}, j_{11}, j_{12}}} \right)_{j_9, j_{10}, j_{11}, j_{12}, j_9, j_{10}, j_{11}, j_{12}}^{(10)}$$

The particle-hole $C_{ij}^{(20)}$ comes from the ring diagram in Fig. 2b, which contains four terms owing to the antisymmetrization specified in Eq. (59),

$$C_{ij}^{(20)} = \Delta(j_1, j_2, j_3, j_4) \Delta(j_1, j_2, j_3, j_4) \Delta(j_5, j_6, j_7, j_8) \Delta(j_5, j_6, j_7, j_8) \sum_{j_9, j_{10}} \sum_{j_{11}, j_{12}} \Delta(j_9, j_{10}, j_{11}, j_{12}) \Delta(j_9, j_{10}, j_{11}, j_{12})$$

$$\times \left(\frac{A_{j_9, j_{10}, j_{11}, j_{12}}^{(20)}}{2j_9+1} \sqrt{1+d_{j_9, j_{10}, j_{11}, j_{12}}} - (-1)^{j_1+j_2+j_3+j_4} A_{j_9, j_{10}, j_{11}, j_{12}}^{(20)} \sqrt{1+d_{j_9, j_{10}, j_{11}, j_{12}}} \right) \left(\frac{A_{j_9, j_{10}, j_{11}, j_{12}}^{(20)}}{2j_9+1} \sqrt{1+d_{j_9, j_{10}, j_{11}, j_{12}}} \right)_{j_9, j_{10}, j_{11}, j_{12}, j_9, j_{10}, j_{11}, j_{12}}^{(20)}$$

$$- (-1)^{j_1+j_2+j_3+j_4} A_{j_9, j_{10}, j_{11}, j_{12}}^{(20)} \sqrt{1+d_{j_9, j_{10}, j_{11}, j_{12}}} \left(\frac{A_{j_9, j_{10}, j_{11}, j_{12}}^{(20)}}{2j_9+1} \sqrt{1+d_{j_9, j_{10}, j_{11}, j_{12}}} \right)_{j_9, j_{10}, j_{11}, j_{12}, j_9, j_{10}, j_{11}, j_{12}}^{(20)}$$

$$+ (-1)^{j_1+j_2+j_3+j_4} A_{j_9, j_{10}, j_{11}, j_{12}}^{(20)} \sqrt{1+d_{j_9, j_{10}, j_{11}, j_{12}}} \left(\frac{A_{j_9, j_{10}, j_{11}, j_{12}}^{(20)}}{2j_9+1} \sqrt{1+d_{j_9, j_{10}, j_{11}, j_{12}}} \right)_{j_9, j_{10}, j_{11}, j_{12}, j_9, j_{10}, j_{11}, j_{12}}^{(20)}$$

Formalism already laid out:
F. Raimondi, CB, arXiv:1709.04330 PRC (2017).

FIG. 5. 1PI, skeleton and interaction irreducible self-energy diagrams appearing at 3rd-order in perturbative expansion (7), making use of the effective hamiltonian of Eq. (9).



Radii and Binding Energies in Oxygen Isotopes: A Challenge for Nuclear Forces

V. Lapoux,^{1,*} V. Somà,¹ C. Barbieri,² H. Hergert,³ J.D. Holt,⁴ and S.R. Stroberg⁴

- New fits of chiral interactions (NNLO_{sat}) highly improve comparison to data

- Deficiencies remain for neutron rich isotopes

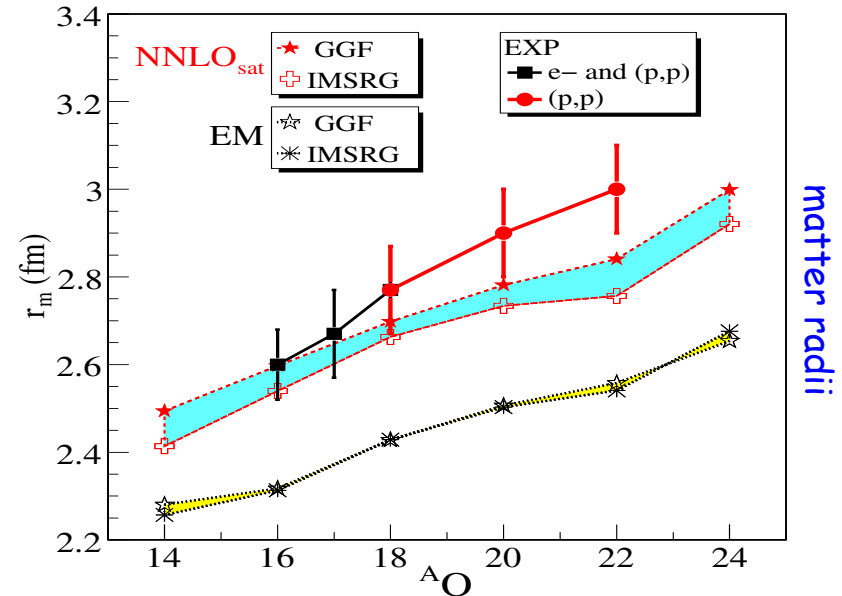
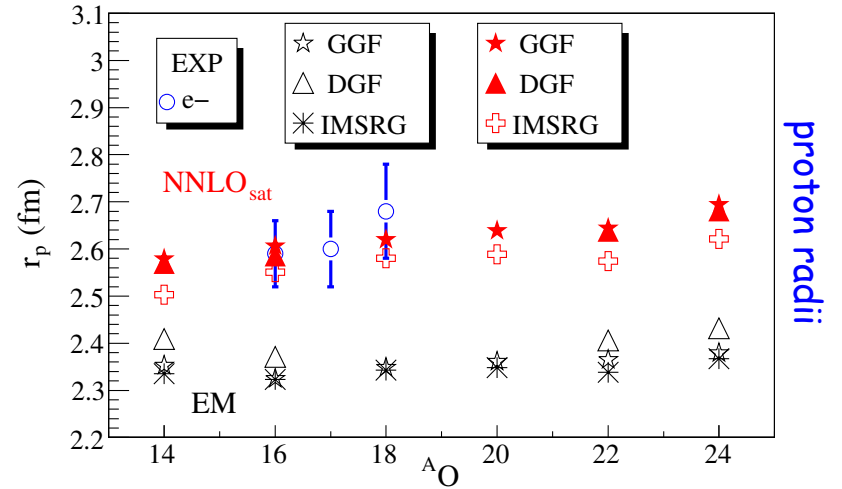
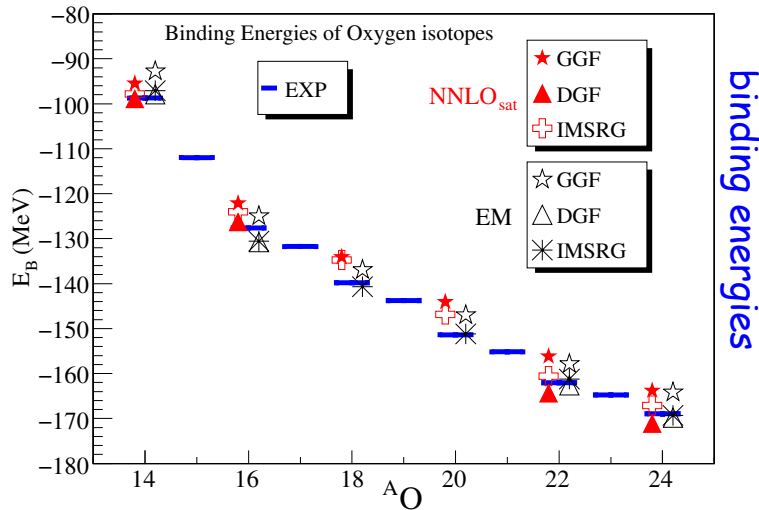
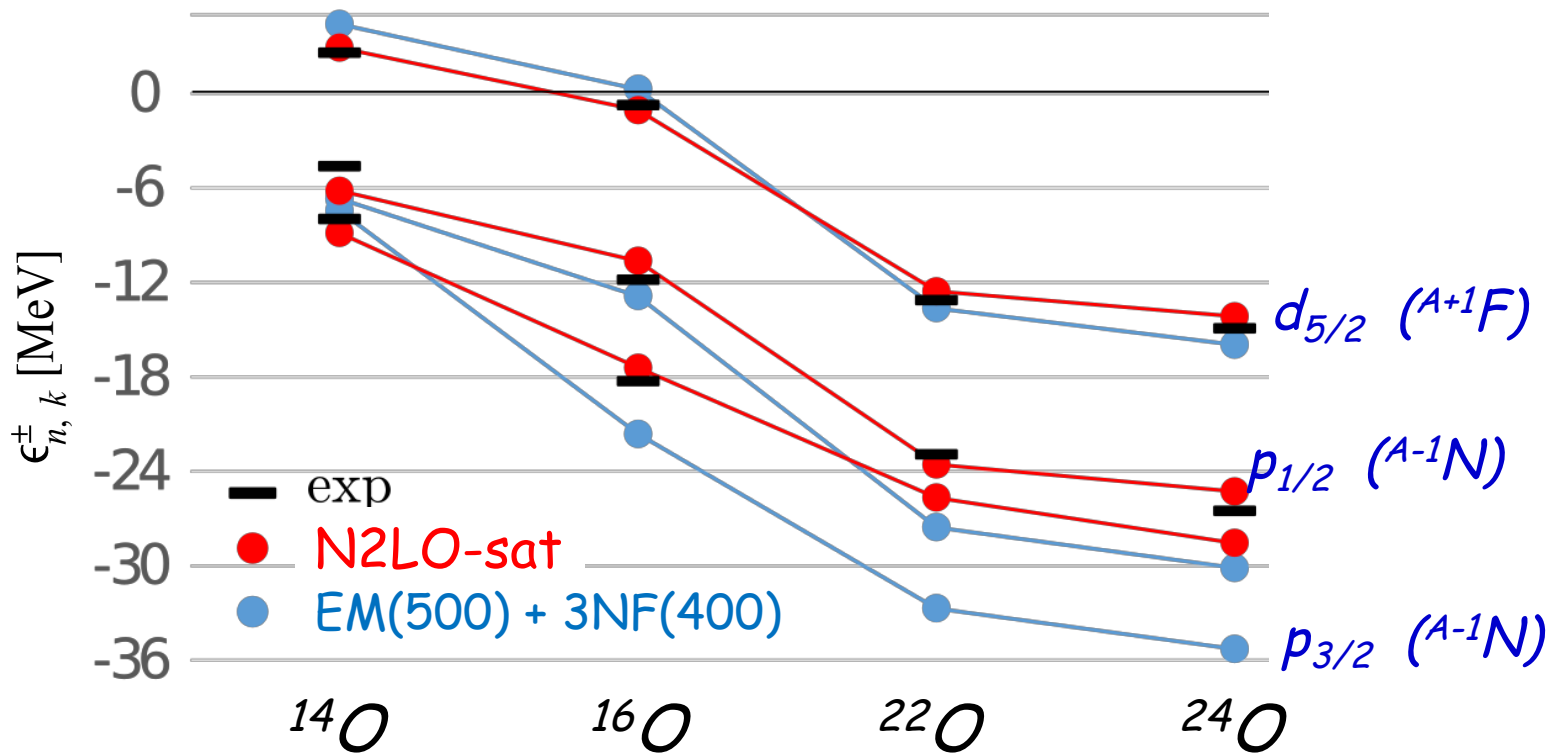


FIG. 1. Oxygen binding energies. Results from SCGF and IMSRG calculations performed with EM [20–22] and NNLO_{sat} [26] interactions are displayed along with available experimental data.

Single particle spectra in Oxygen

A. Cipollone, CB, P. Navrátil, Phys. Rev. Lett. **111**, 062501 (2013)
and Phys. Rev. C **92**, 014306 (2015)
and *in preparation*

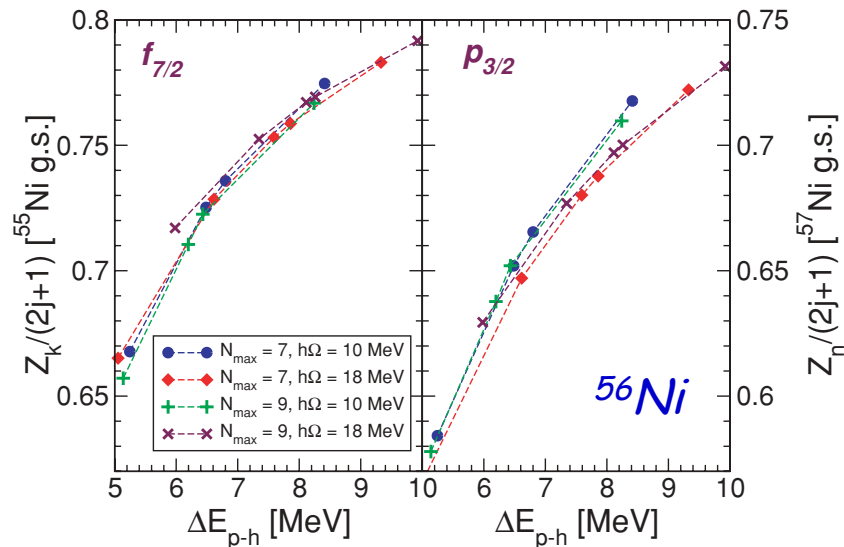


Z/N asymmetry dependence of SFs - Theory

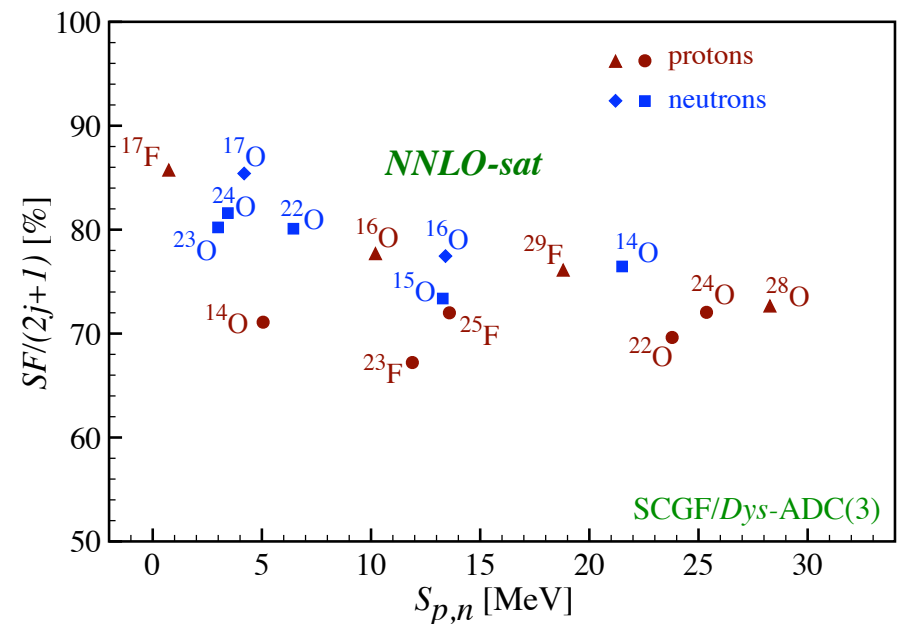
Ab-initio calculations explain (a very weak) the Z/N dependence but the effect is much lower than suggested by direct knockout

Rather the quenching is high correlated to the gap at the Femi surface.

Spectroscopic factor are strongly correlated to p-h gaps:



CB, M. Hjorth-Jensen,
Phys. Rev. C **79**, 064313 (2009)



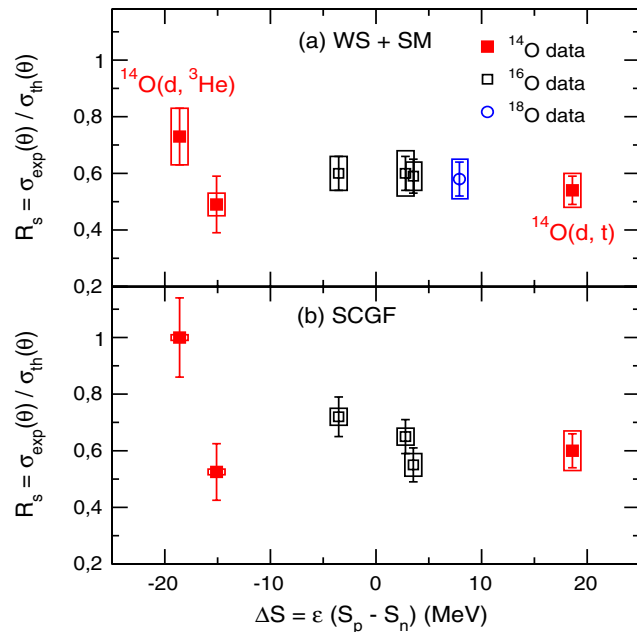
A. Cipollone, CB, P Navrátil, Phys. Rev. C **92**, 014306 (2015)
and CB, unpublished (2016)

Z/N asymmetry dependence of SFs

Calculated spectroscopic factors are found to be:

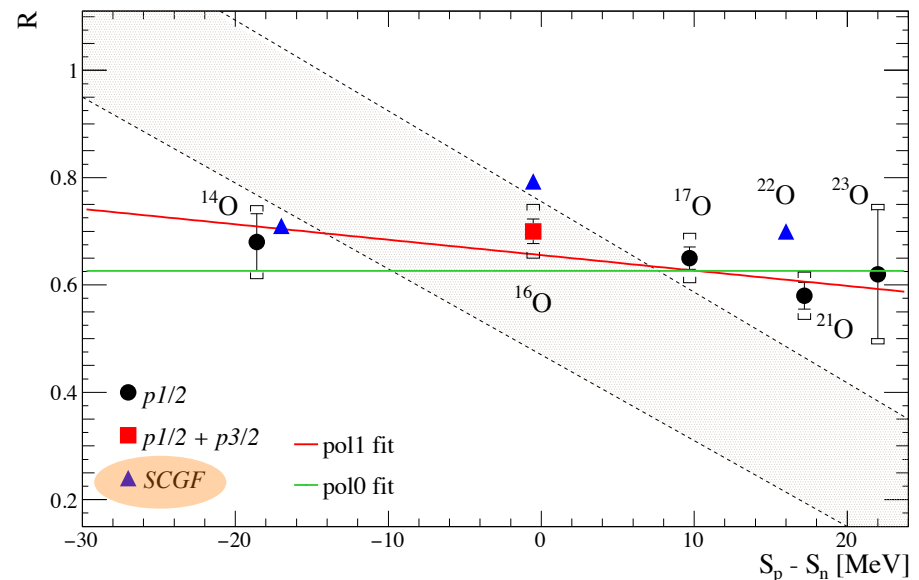
- correlated to p-h gaps
- independent of asymmetry
- consistent with experimental data

$^{14}\text{O}(d,t)^{13}\text{O}$ and $^{14}\text{O}(d,^3\text{He})^{13}\text{N}$
transfer reactions @ SPIRAL



[F. Flavigny et al, PRL110, 122503 (2013)]

$A\text{O}(p,2p)^{A-1}\text{N}$ at GSI (R³B-LAND)



Proton SF for $^{16}\text{O} \rightarrow ^{15}\text{N}$:

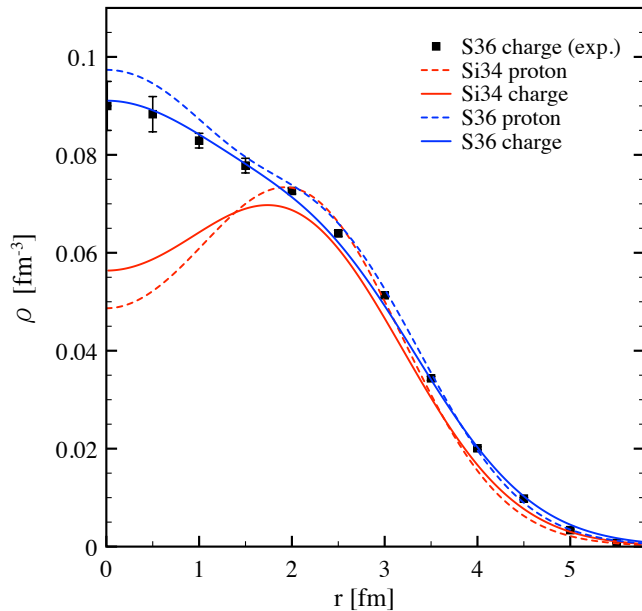
$p_{1/2}$: 0.78 (SCGF) 0.80 (exp.)
 $p_{3/2}$: 0.80 (SCGF) 0.65 (exp. – up to cont.)

L. Atar, et al., in preparation (2017) – see talk by T. Aumann

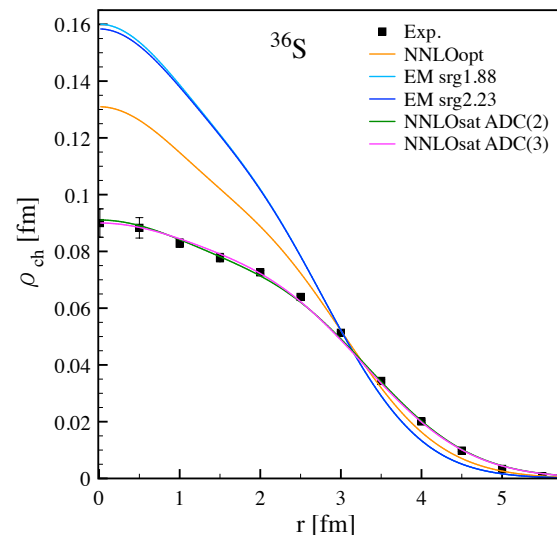
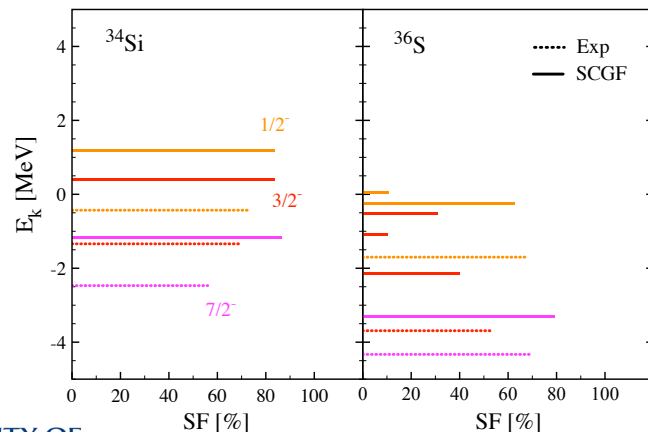
Bubble nuclei... ^{34}Si prediction

Duguet, Somà, Lecuse, CB, Navrátil,
Phys.Rev. C95, 034319 (2017)

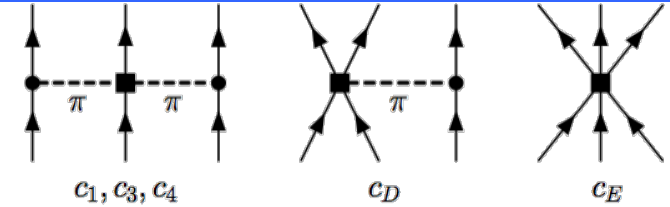
- ^{34}Si is unstable, charge distribution is still unknown
- Suggested central depletion from mean-field simulations
- *Ab-initio* theory confirms predictions



Validated by charge distributions and neutron quasiparticle spectra:



- Local: chiral N³LO NN+ N²LO 3N500
 - $c_D = -0.2$ $c_E = -0.205$ (${}^3\text{H } E_{\text{gs}} = -8.48$ MeV)
 - ${}^4\text{He}$



$$\langle H \rangle = -28.4939 \quad \langle V_{3b_2\pi} \rangle = -5.8819 \quad \langle V_{3b_D} \rangle = -0.2206 \quad \langle V_{3b_E} \rangle = 1.2665$$

- Non-local: chiral N²LO_{sat} NN+3N
 - $c_D = +0.8168$ $c_E = -0.0396$ (${}^3\text{H } E_{\text{gs}} = -8.53$ MeV)
 - ${}^4\text{He}$

$$\langle H \rangle = -28.4596 \quad \langle V_{3b_2\pi} \rangle = -4.7260 \quad \langle V_{3b_D} \rangle = 1.3897 \quad \langle V_{3b_E} \rangle = 0.4174$$

- Local/Non-local: chiral N³LO NN+ N²LO

$$F\left(\frac{1}{2}(\pi_1^2 + \pi_2^2); \Lambda_{\text{nonloc}}\right) W_1^Q(\Lambda_{\text{loc}}) F\left(\frac{1}{2}(\pi_1^2 + \pi_2^2); \Lambda_{\text{nonloc}}\right)$$

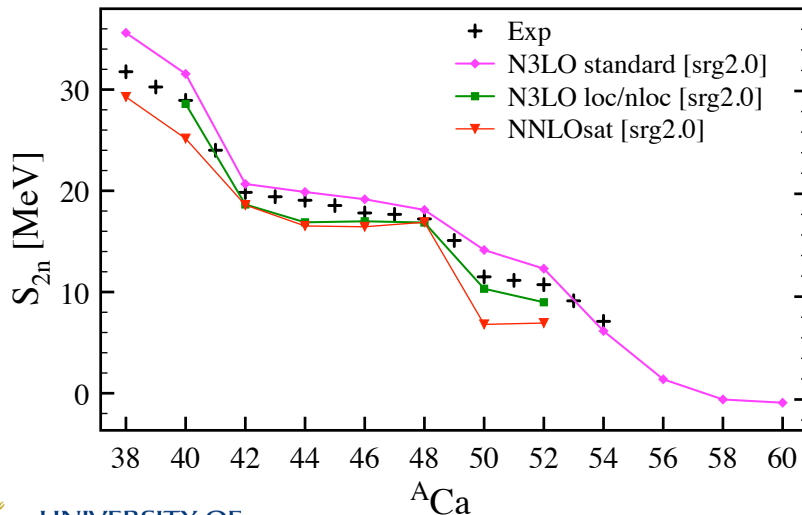
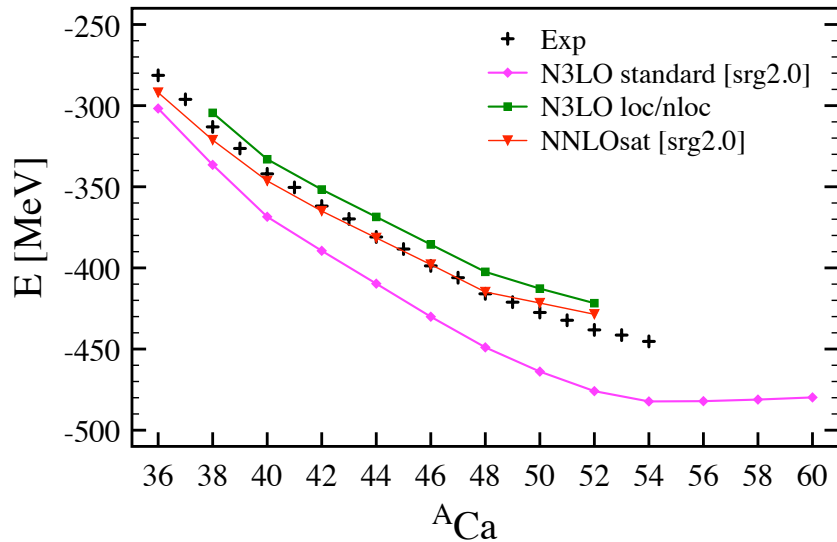
Use completeness in HO basis to calculate products of $F W F$

- $c_D = +0.7$ $c_E = -0.06$ (${}^3\text{H } E_{\text{gs}} = -8.44$ MeV)
- ${}^4\text{He}$

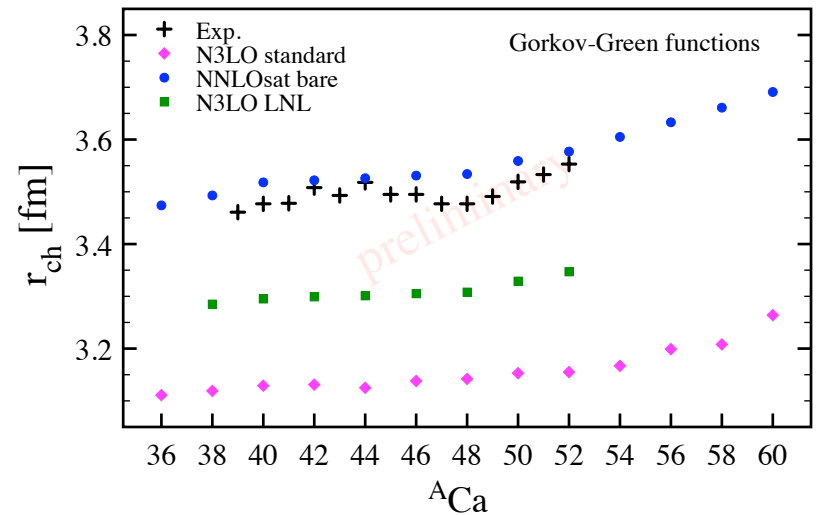
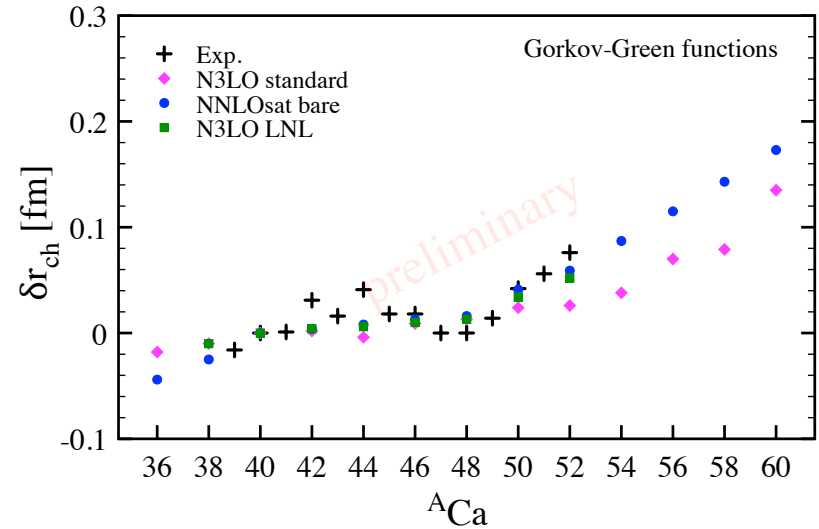
$$\langle H \rangle = -28.2530 \quad \langle V_{3b_2\pi} \rangle = -4.8124 \quad \langle V_{3b_D} \rangle = 0.7414 \quad \langle V_{3b_E} \rangle = 0.4255$$

N3LO(500) + nln 3NF

SCGF – Gorkov-ADC(2)



PRELIMINARY



Masses in the Ti isotopic chain

- High precision measurements at TITAN (TRIUMF):
Newly developed Multiple-Reflection Time-of-Flight
Mass Spectrometer (MR-TOF-MS)
- Weak shell closure at N=32 (quenched w.r.t. ^{52}Ca)

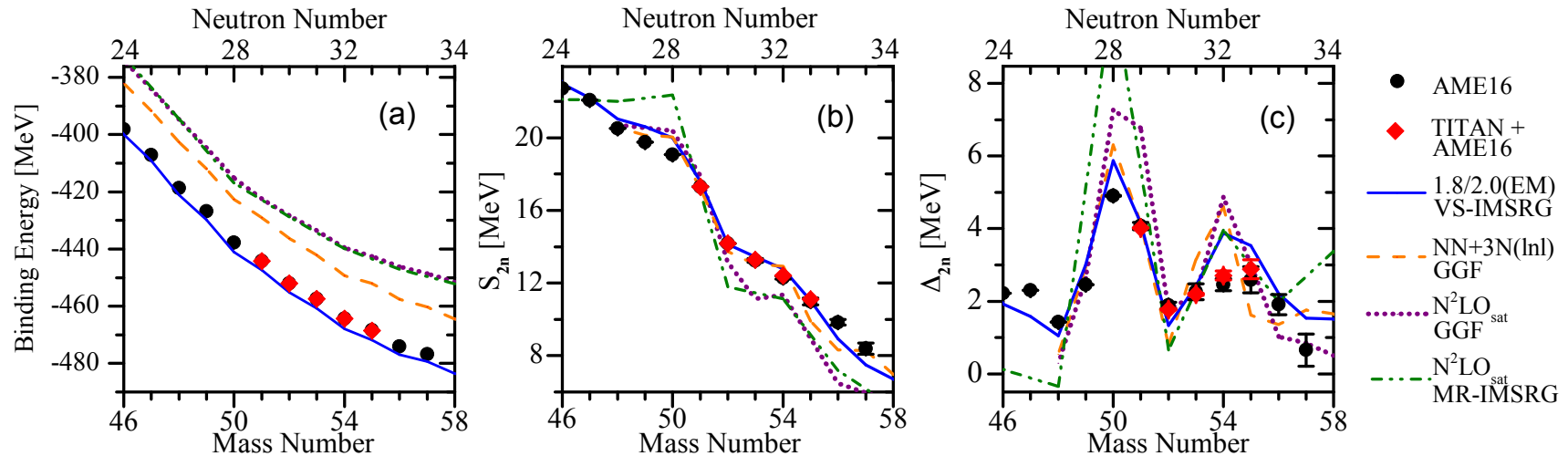
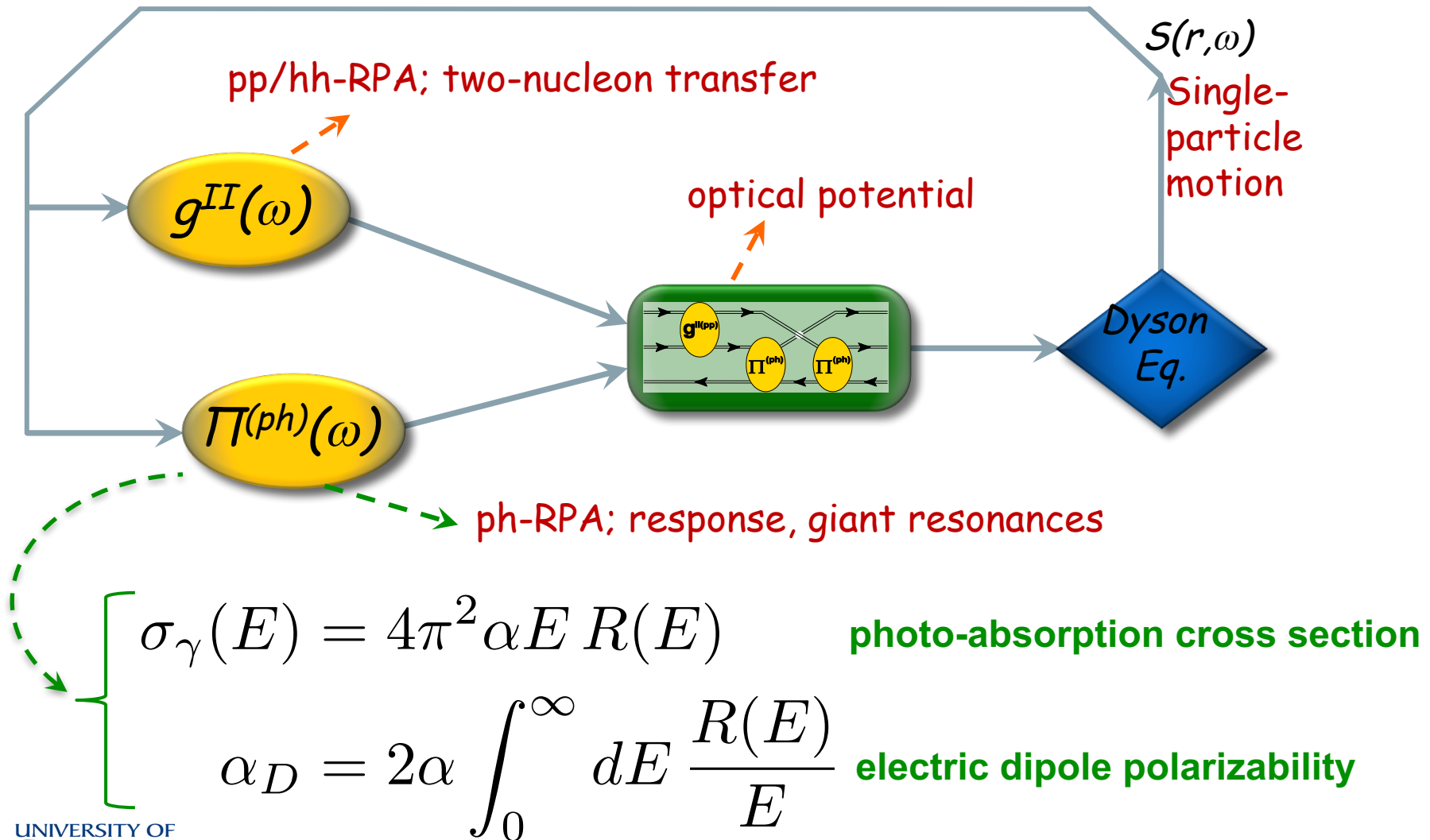


FIG. 4. The mass landscape of titanium isotopes is shown from three perspectives: (a) absolute masses (shown in binding energy format), (b) its first “derivative” as two-neutron separation energies (S_{2n}), and (c) its second “derivative” as empirical neutron-shell gaps (Δ_{2n}). Both theoretical *ab-initio* calculations (lines) and experimental values (points) are shown.

E. Leistenschneider *et al.*, [arXiv:1710.08537](https://arxiv.org/abs/1710.08537) (2017) – **TITAN** coll. @ TRIUMF

Electromagnetic response in SCGF

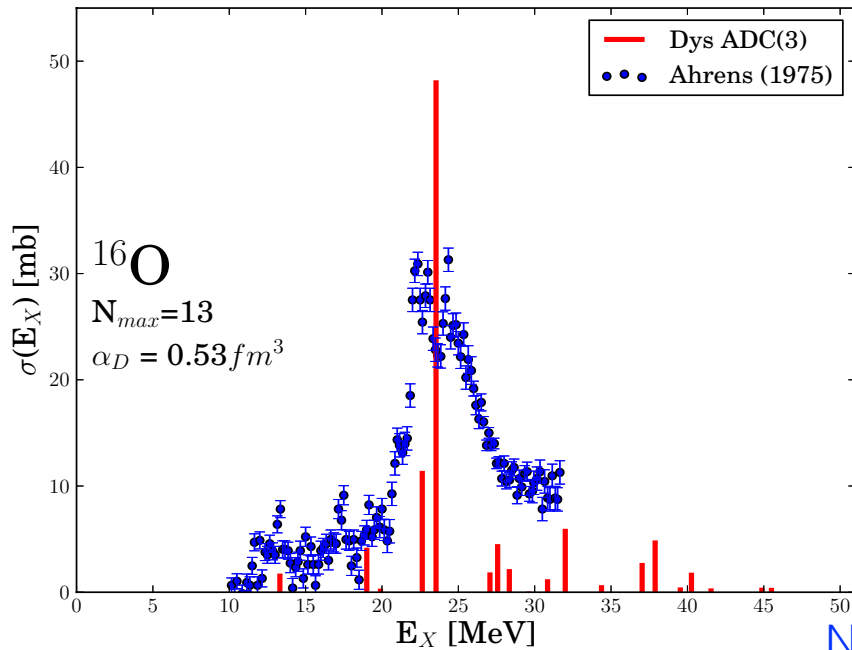


$$\sigma_{\gamma}(E) = 4\pi^2 \alpha E R(E)$$

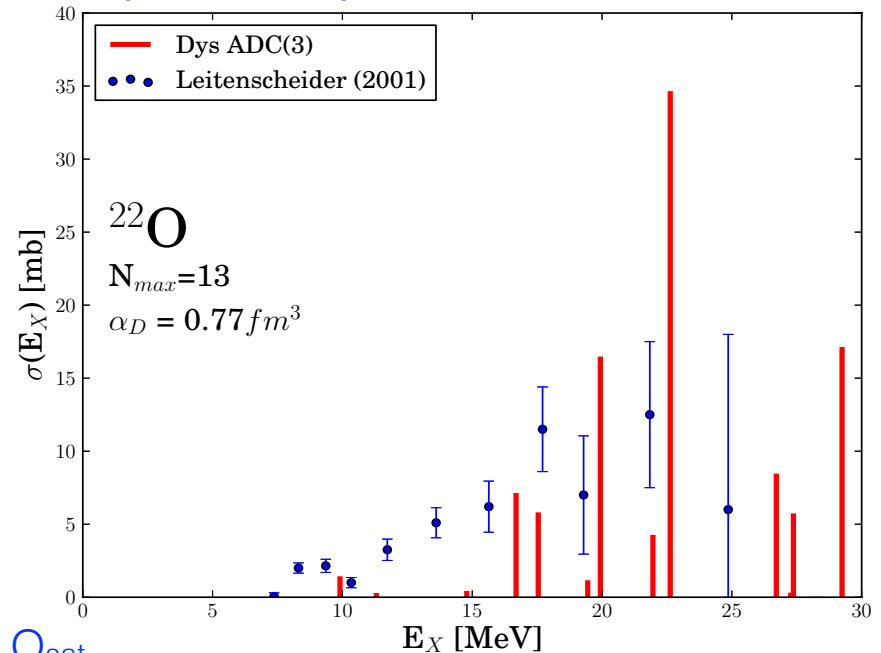
$$\alpha_D = 2\alpha \int_0^{\infty} dE \frac{R(E)}{E}$$

Results for Oxygen isotopes

σ from RPA response (discretized spectrum) vs σ from photoabsorption and Coulomb excitation



NNLO_{sat}



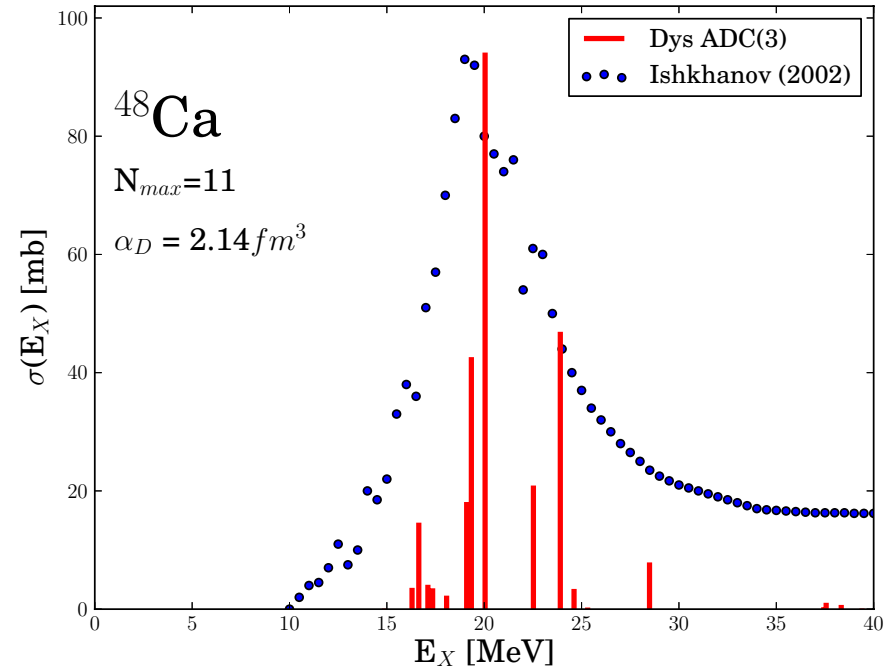
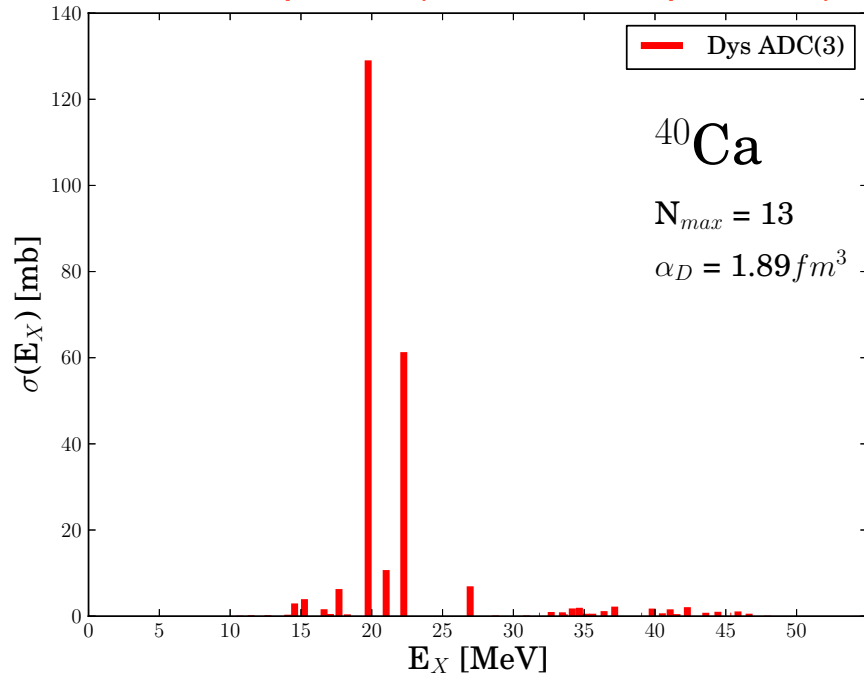
- GDR position of ^{16}O reproduced
- Hint of a soft dipole mode on the neutron-rich isotope

Nucleus	Dipole polarizability α_D (fm^3)		
	SCGF	CC/LIT	Exp
^{16}O	0.53	0.57(1)	0.585(9)
^{22}O	0.77	0.86(4)	0.43(4)

Slides courtesy of F. Raimondi - TRIUMF wks, Mar 2017

Results for Calcium isotopes

σ from RPA response (discretized spectrum) vs σ from photoabsorption and Coulomb excitation



NNLO_{sat}

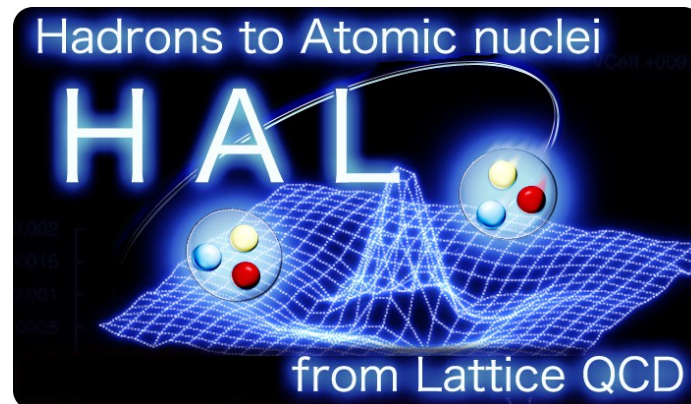
- GDR positions reproduced

Nucleus	Dipole polarizability α_D (fm^3)		
	SCGF	CC/LIT	Exp
^{40}Ca	1.89	1.47 (1.87) _{thresh}	1.87(3)
^{48}Ca	2.14	2.45	2.07(22)

Slides courtesy of F. Raimondi - TRIUMF wks, Mar 2017

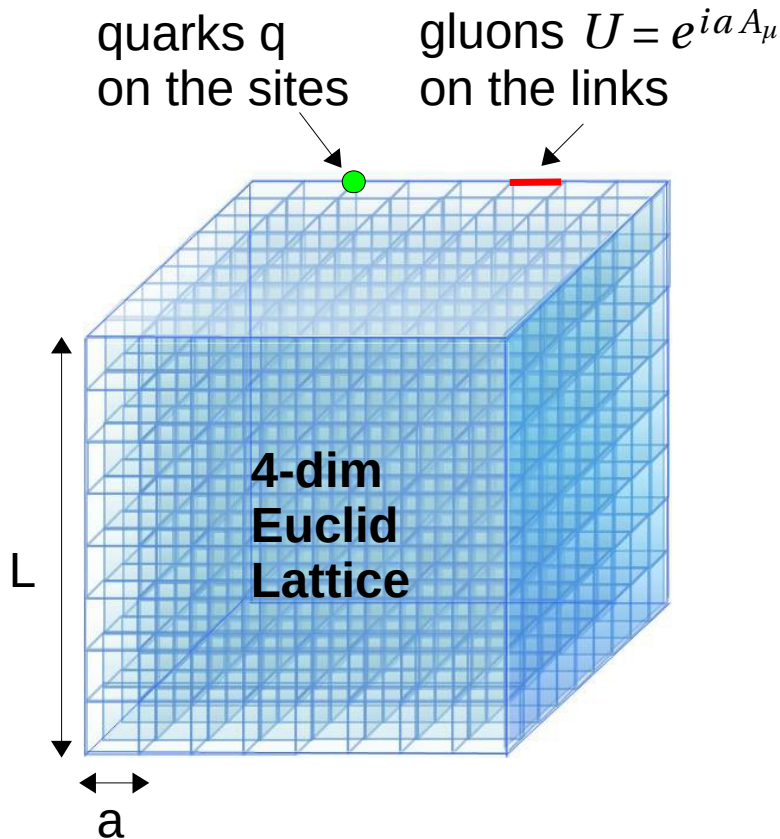
Study of nuclear interactions from Lattice QCD

In collaboration with:



Lattice QCD

$$L = -\frac{1}{4} G_{\mu\nu}^a G_a^{\mu\nu} + \bar{q} \gamma^\mu (i \partial_\mu - g t^a A_\mu^a) q - m \bar{q} q$$



Vacuum expectation value

$$\begin{aligned} & \langle O(\bar{q}, q, U) \rangle \\ &= \int dU d\bar{q} dq e^{-S(\bar{q}, q, U)} O(\bar{q}, q, U) \\ &= \int dU \det D(U) e^{-S_U(U)} O(D^{-1}(U)) \\ &= \lim_{N \rightarrow \infty} \frac{1}{N} \sum_{i=1}^N O(D^{-1}(U_i)) \end{aligned}$$

path integral

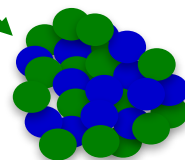
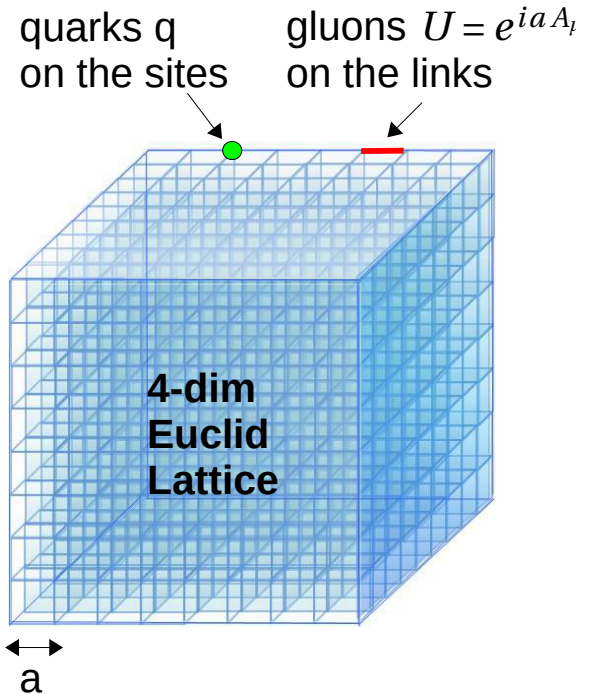
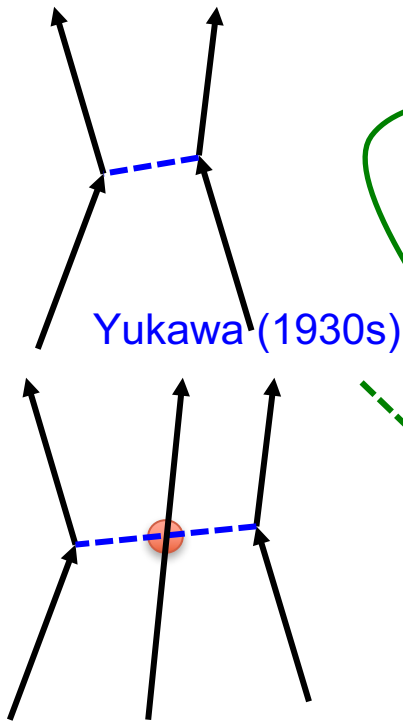
quark propagator

$\{ U_i \}$: ensemble of gauge conf. U
generated w/ probability $\det D(U) e^{-S_U(U)}$

- ★ Well defined (regularized)
- ★ Manifest gauge invariance
- ★ Fully non-perturbative
- ★ Highly predictive

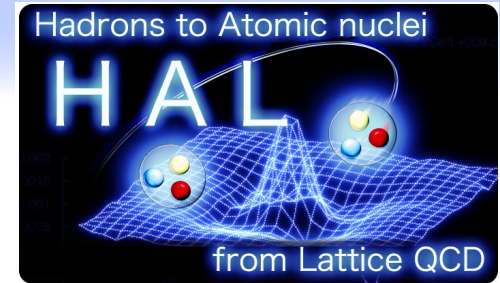
Approaches to nuclei from LQCD

$$L = -\frac{1}{4} G_{\mu\nu}^a G_a^{\mu\nu} + \bar{q} \gamma^\mu (i \partial_\mu - g t^a A_\mu^a) q - m \bar{q} q$$



Nucleus

Why nuclear interactions on the Lattice??

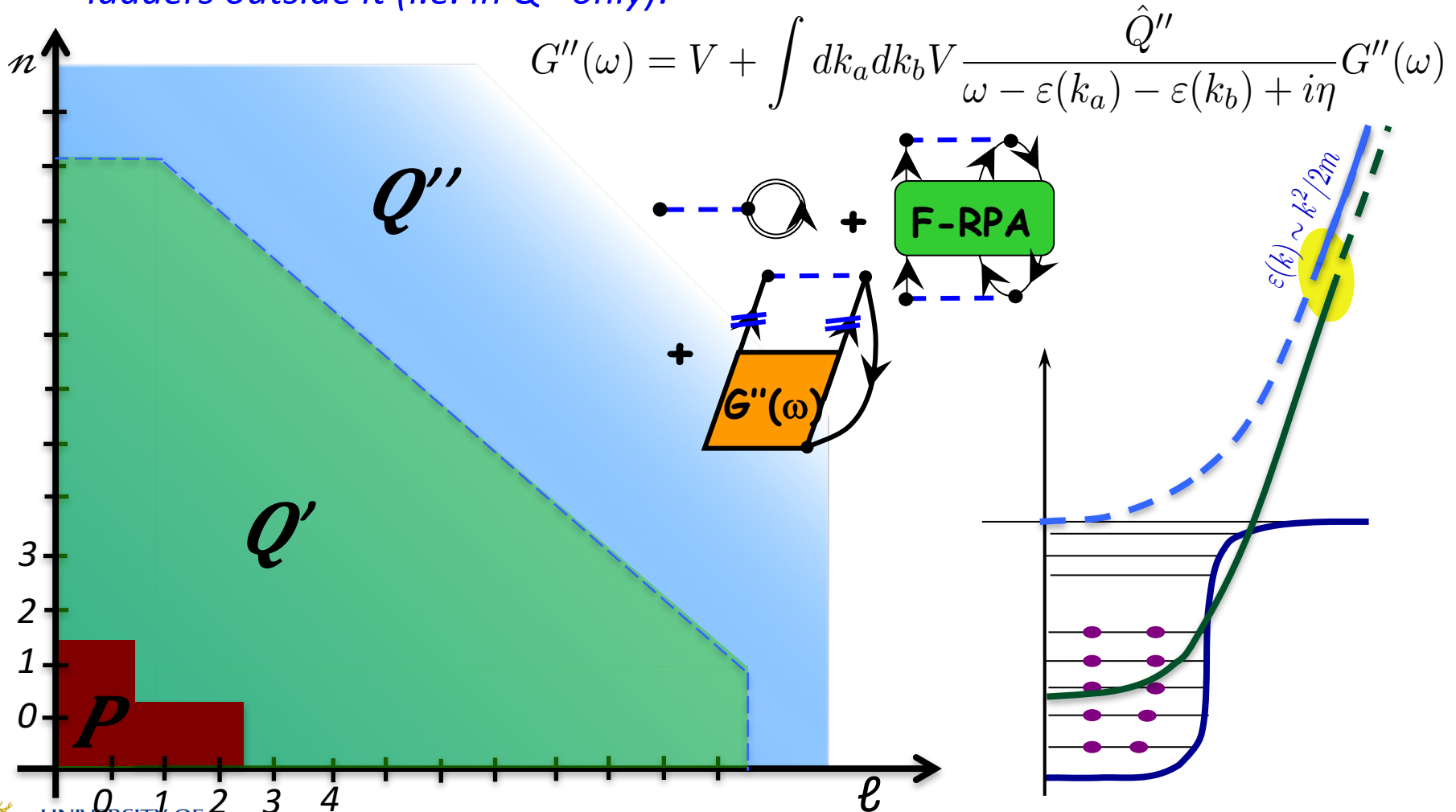


- *Extend LQCD beyond few-bodies*
- *Reproduces exactly scattering and NN, 3N, observables that would be computed with Lattice QCD.*
- *Not based on a specific EFT momentum scale*
 → exploitable to high densities (e.g. Neutron stars)
- *No LECs to worry about ...AND:*
- *Variation in potentials from variation in sink operators (→ estimation of theoretical uncertainties, missing N-body terms, etc...)*
- *Direct derivation of hyperon-nucleon interactions*
- *3NF can be derived consistently with NN interactions*

→ Need to develop appropriate many-body methods

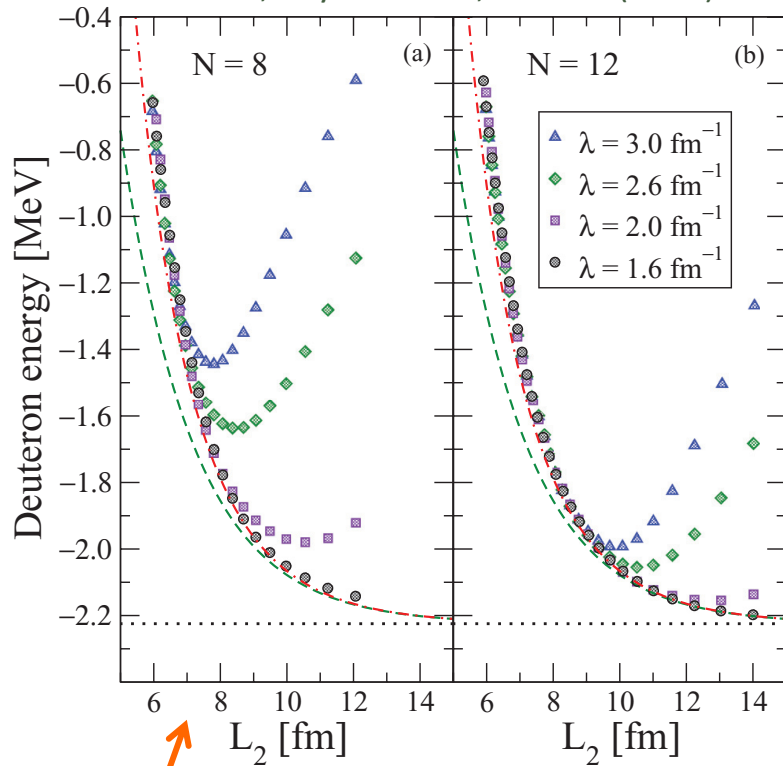
Mixed SCGF-Brueckner approach

Solve full many-body dynamics in model space ($P+Q'$) and the Goldstone's ladders outside it (i.e. in Q'' only):

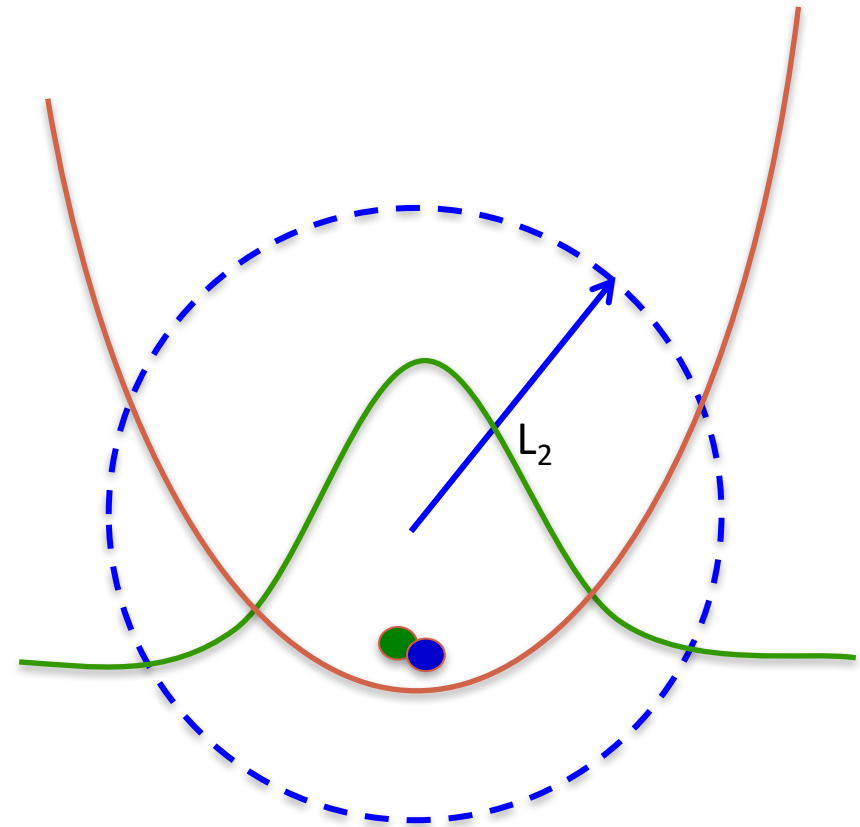


Infrared convergence

Moore et al., Phys. Rev. C87, 044326 (2013)



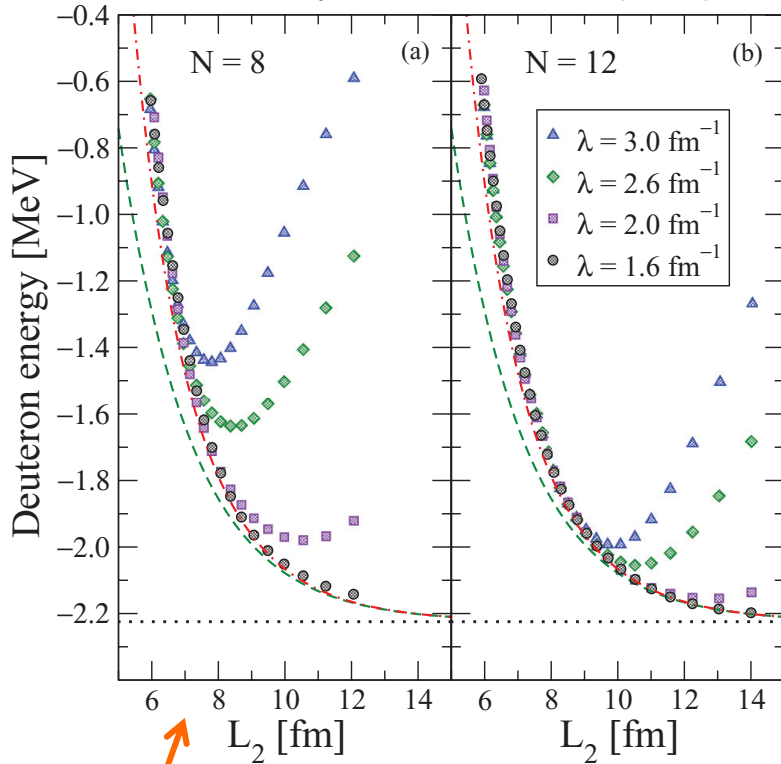
Deuteron g.s. Energy
EM(500) – N3LO two-nucleon force



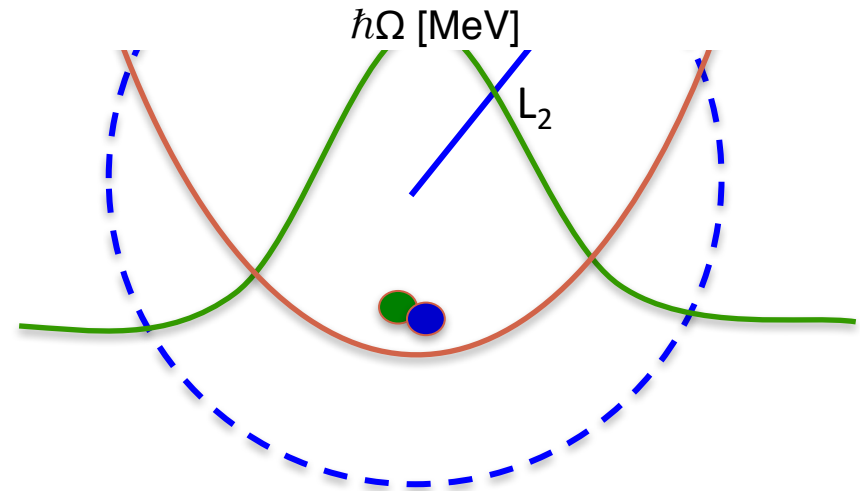
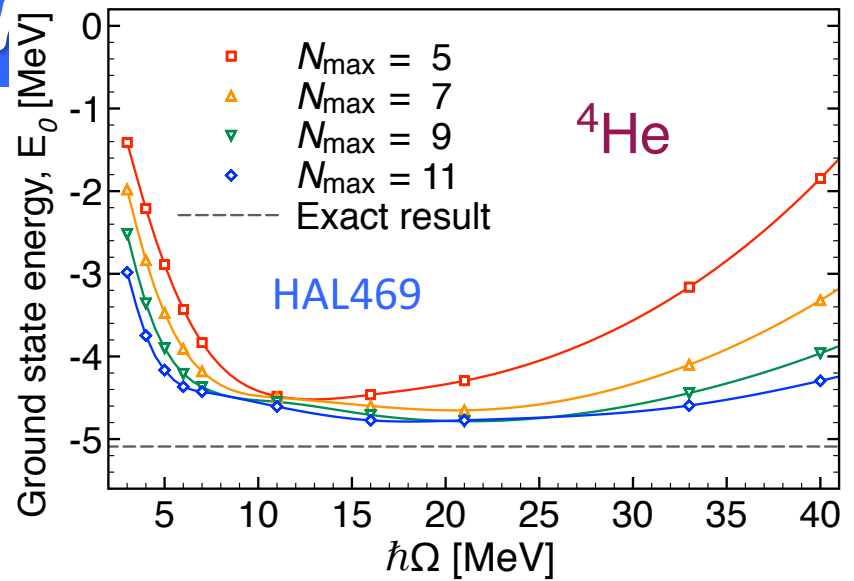
$$L_2 = \sqrt{2(N + 3/2 + 2)}b$$

Infrared convergence

Moore et al., *Phy. Rev. C* **87**, 044326 (2013)



Deuteron g.s. Energy
EM(500) – N3LO two-nucleon force

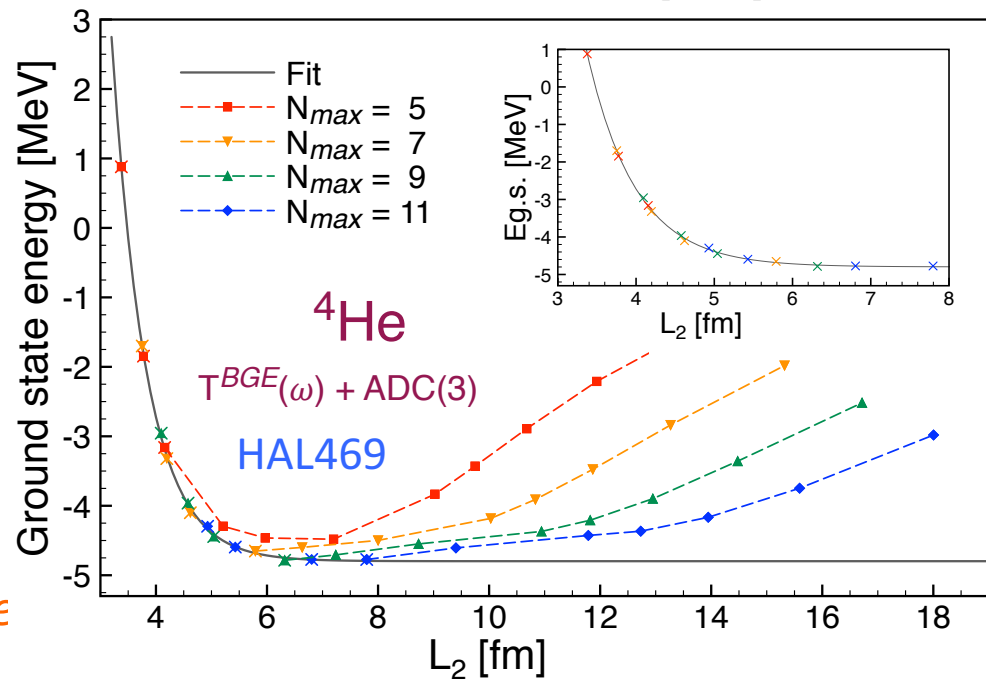
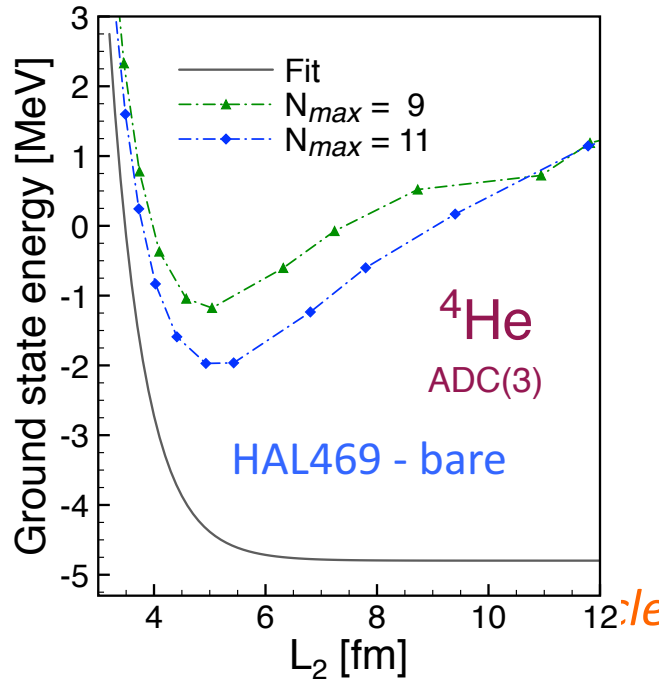
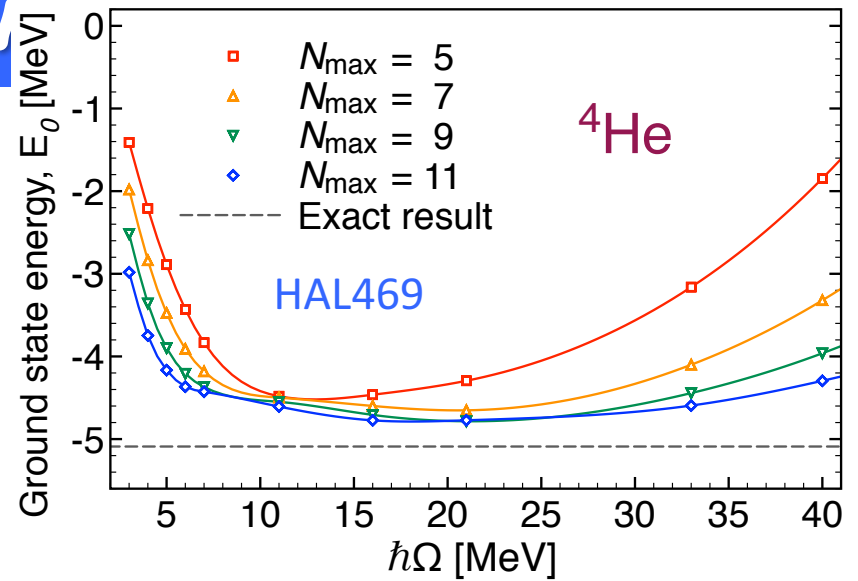


$$L_2 = \sqrt{2(N + 3/2 + 2)}b$$

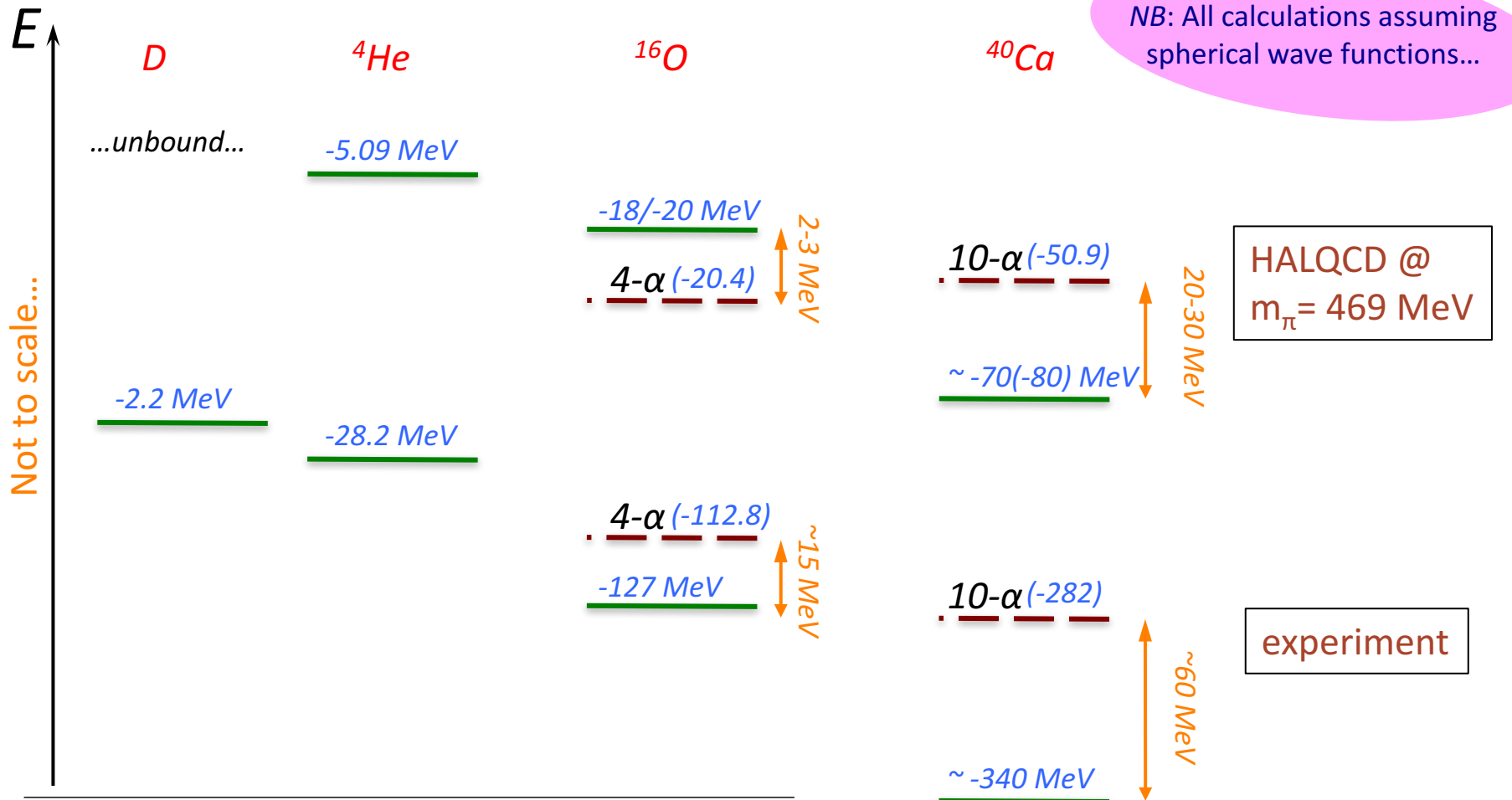
Infrared convergence

Short-range repulsion in the HALQCD-type potentials can be tamed correctly even for large nuclei.

C. McIlroy, CB, et al., arXiv:1701.02607 [nucl-th]

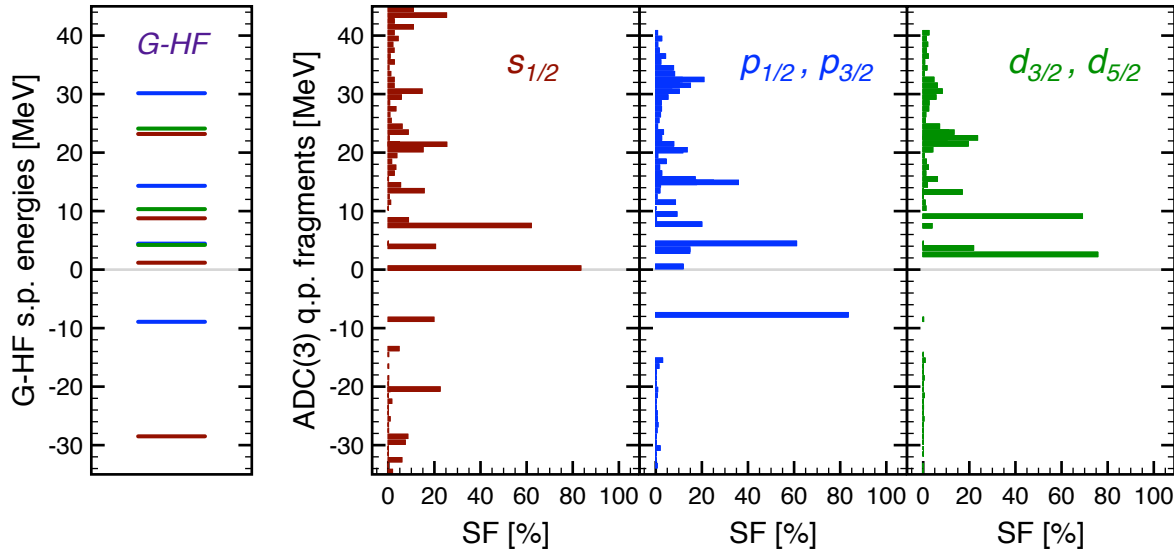


Results for binding



E_0^A [MeV]	${}^4\text{He}$	${}^{16}\text{O}$	${}^{40}\text{Ca}$
BHF [22]	-8.1	-34.7	-112.7
$G(\omega) + \text{ADC}(3)$	-4.80(0.03)	-17.9 (0.3) (1.8)	-75.4 (6.7) (7.5)
Exact Result [51]	-5.09	-	-
Separation into ${}^4\text{He}$ clusters:	-	-2.46 (0.3) (1.8)	24.5 (6.7) (7.5)

Spectral strength in ^{16}O and ^{40}Ca :

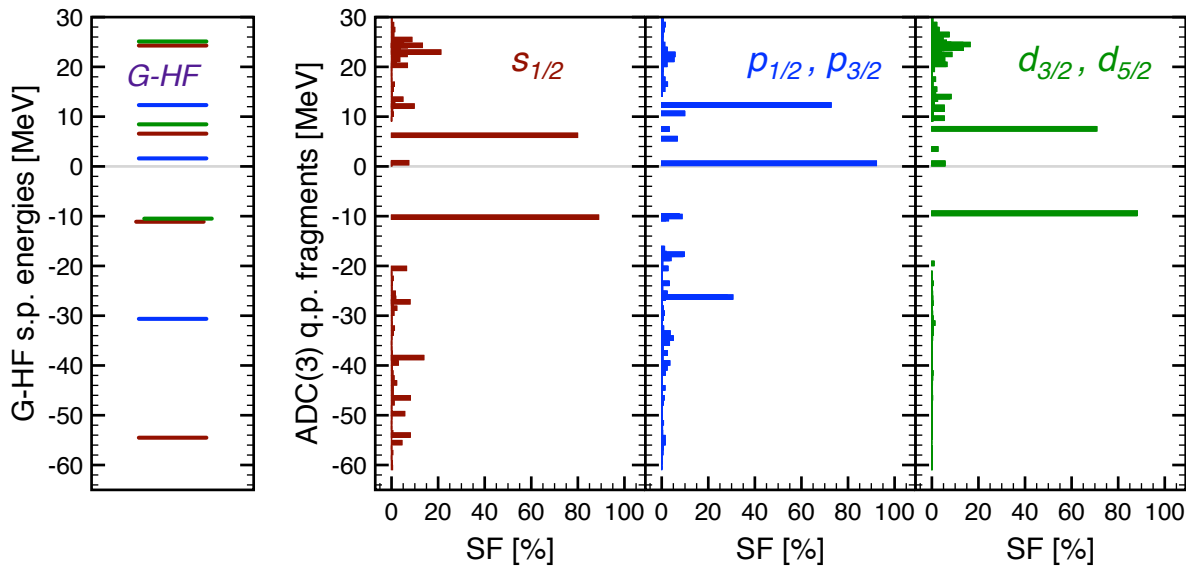


Particle-hole gaps:

^{16}O

$m_\pi = 469$ MeV: ~ 8 MeV

Expt (phys m_π): 11.5 MeV



^{40}Ca

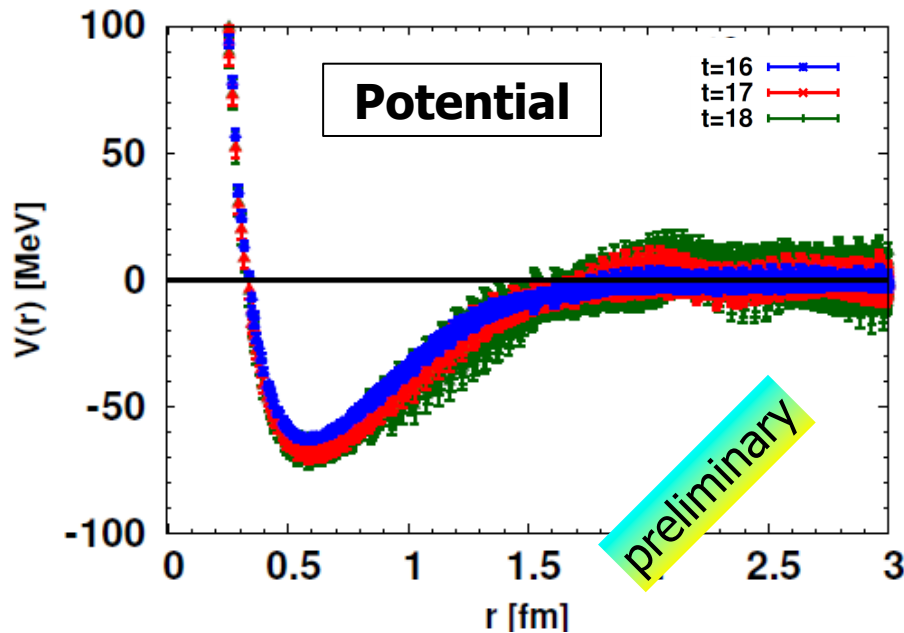
$m_\pi = 469$ MeV: ~ 10 MeV

Expt (phys m_π): 7.5 MeV

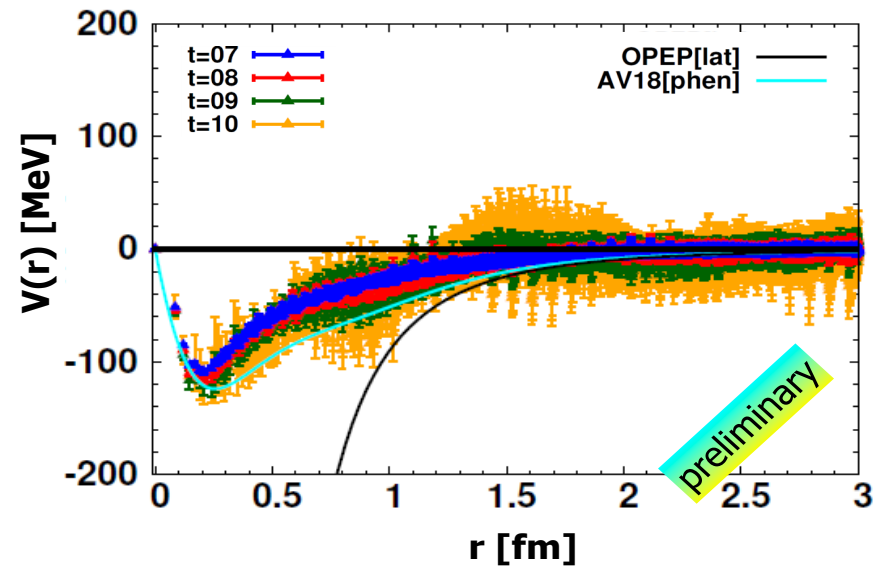
Future application for Ys in nuclei now possible

- Physical mass now under reach ($m_\pi \approx 145$ MeV) for hyperons
- Need to improve on statistic for the NN sector

$\Omega\Omega$ potential



$NN(^3S_1)$ tensor potential



HALQCD coll. -- Talk of **S. Aoki** at Kavli institute, Oct. 2016

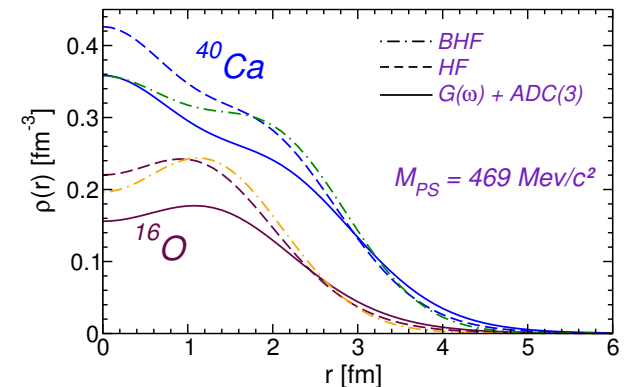
Summary

Mid-masses and chiral interactions:

- Leading order 3NF are crucial to predict many important features that are observed experimentally (drip lines, saturation, orbit evolution, etc...)
- New fits of chiral interaction are promising for low-energy observables and for scattering - mass/radii/spectroscopy are improved but there remain issues (symm energy, neutron rich) and dependency on LEC/cutoffs.
- Ab initio optical potentials (nucleon-nucleus) within reach.
- Dipole responses and polarizabilities, are reproduced well at (LO) RPA .
- Effective charges can be computed for SM applications

HALQCD Nuclear forces:

- Strong short range behavior calls for new ideas in *ab-initio* many-body methods. Diagram resummation through *G*-matrix is good starting point (to be extended).
- At $m_\pi=469\text{MeV}$, closed shell 4He , 16O and 40Ca are bound. But oxygen is unstable toward $4\text{-}\alpha$ break up, calcium stays bound.



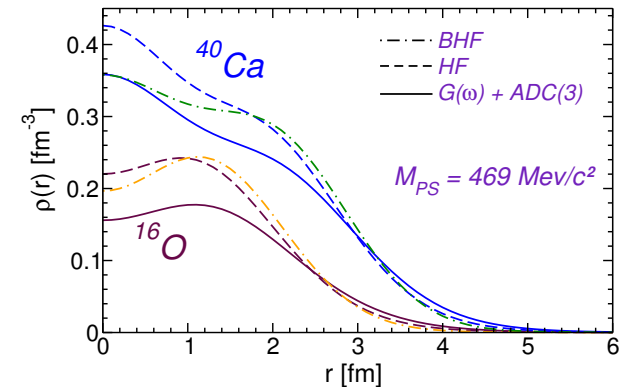
Summary

Mid-masses and chiral interactions:

- Leading order 3NF are crucial to predict many important features that are observed experimentally (drip lines, saturation, orbit evolution, etc...)
- New fits of chiral interaction are promising for low-energy observables and for scattering - mass/radii/spectroscopy are improved but there remain issues (symm energy, neutron rich) and dependency on LEC/cutoffs.
- Ab initio optical potentials (nucleon-nucleus) within reach.
- Dipole responses and polarizabilities, are reproduced well at (LO) RPA .
- Effective charges can be computed for SM applications

HALQCD Nuclear forces:

- Strong short range behavior calls for new ideas in *ab-initio* many-body methods. Diagram resummation through *G*-matrix is good starting point (to be extended).
- At $m_\pi=469\text{MeV}$, closed shell 4He , 16O and 40Ca are bound. But oxygen is unstable toward $4\text{-}\alpha$ break up, calcium stays bound.



Thank you for your attention!!!

Thanks to all collaborators!!

...and thank you for your attention!!!



A. Cipollone, C. McIlroy
A. Rios, A. Idini, F. Raimondi



A. Polls



V. Somà, T. Duguet



W.H. Dickhoff,
S. Waldecker

energie atomique • energies alternatives

ECT*

EUROPEAN CENTRE FOR THEORETICAL STUDIES
IN NUCLEAR PHYSICS AND RELATED AREAS

A. Carbone



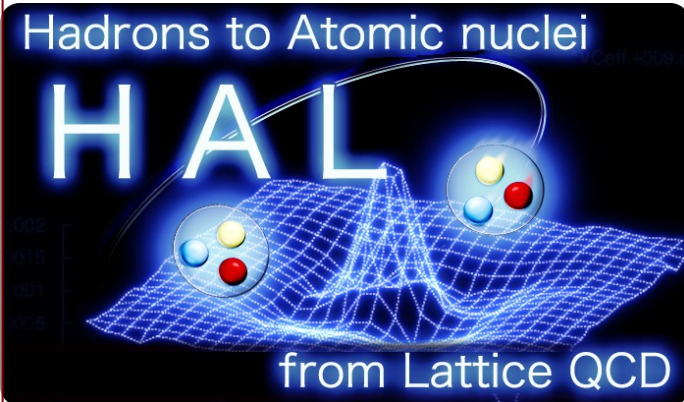
D. Van Neck



P. Navratil



M. Hjorth-Jensen

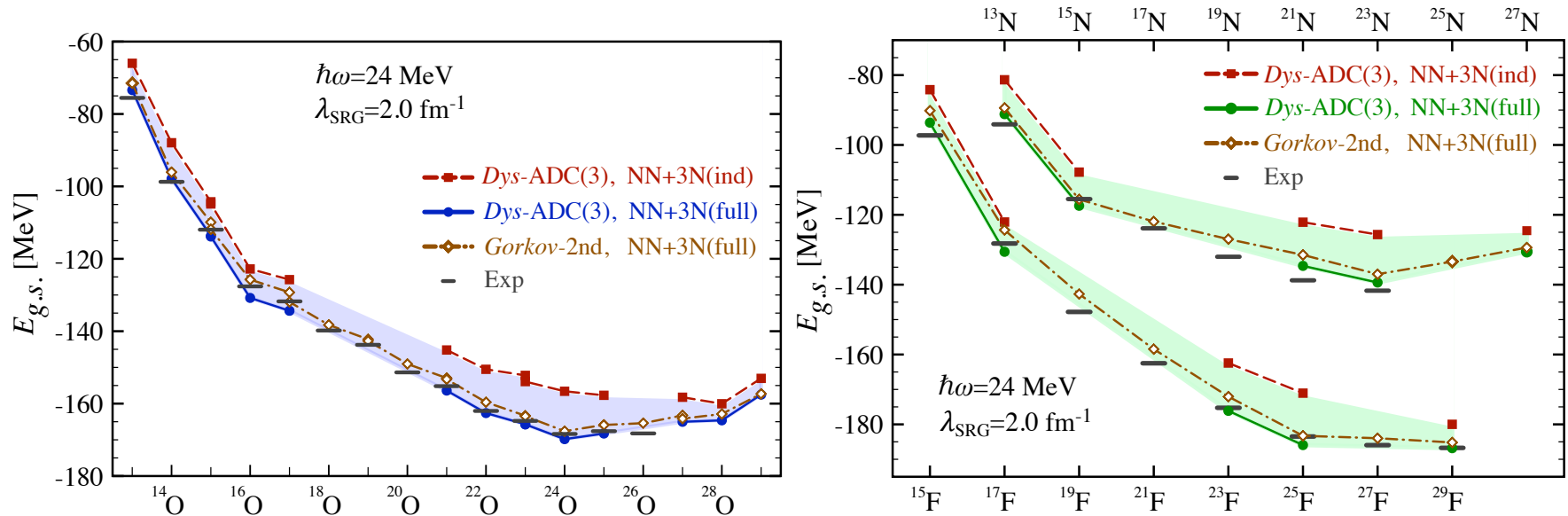


S. Aoki,
T. Doi, T. Hatsuda, Y. Ikeda,
T. Inoue,
N. Ishii, K. Murano,
H. Nemura, K. Sasaki
F. Etminan
T. Miyamoto,
T. Iritani
S. Gongyo

YITP Kyoto Univ.
RIKEN Nishina
Nihon Univ.
RCNP Osaka Univ
Univ. Tsukuba
Univ. Birjand
Univ. Tsukuba
Stony Brook Univ.
YITP Kyoto Univ.

Results for the N-O-F chains

A. Cipollone, CB, P. Navrátil, Phys. Rev. Lett. **111**, 062501 (2013)
and Phys. Rev. C **92**, 014306 (2015)



→ 3NF crucial for reproducing binding energies and driplines around oxygen

→ cf. microscopic shell model [Otsuka et al, PRL**105**, 032501 (2010).]